# LOW COMPLEXITY EXTENSIONS OF NON-LINEAR MAPPINGS

by

Iñaki Iglesias

A thesis submitted to the Faculty of the University of Delaware in partial fulfillment of the requirements for the degree of Master of Science in Electrical and Computer Engineering

Summer 2014

**LOW COMPLEXITY EXTENSIONS OF NON-LINEAR MAPPINGS**

by

Iñaki Iglesias

Approved: _____
Javier Garcia-Frias, Ph.D.
Professor in charge of thesis on behalf of the Advisory Committee

Approved: _____
Kenneth E. Barner, Ph.D.
Chair of the Department of Electrical and Computer Engineering

Approved: _____
Babatunde A. Ogunnaike, Ph.D.
Dean of the College of Engineering

Approved: _____
James G. Richards, Ph.D.
Vice Provost for Graduate and Professional Education

## ACKNOWLEDGMENTS

First of all, I would like to thank my advisor, Professor Javier García Frías, for the opportunity of working with him throughout these years. His passion for engineering and hardworking attitude have influenced me in a greatly manner and his support at the tough moments is something I do not intend to forget. I feel that researching under his guidance has been an enriching life experience and I feel very thankful for that.

Second, I am very grateful to "la Caixa" savings bank for their outstanding graduate fellowship program and for giving me the chance to take my academic career to a higher stage with their generous economical help.

On a more personal note, I need to mention my great officemates Kejing Liu and Bo Lu for all the good times we shared together; I really hope there are many more to come. Special thanks to Luisa Polanía, Qi Wang, Guillermo Costa, Juris Pupcenoks and Carlos Reyes for their unique way of showing friendship and adding so many highlights to my stay in Delaware. Also many thanks to Bob and Mary Hawthorne for making a place I will remember forever out of 110 Mulberry Road.

Finally, my deepest gratitude goes to Álvaro González and Iñaki Esnaola. They have aided me during so many stages, assisted me with so many problems, lead me through so many paths and inspired me in so many ways that I feel this thesis could only be dedicated to them. *Eskerrik asko, bihotz-bihotzez.*

## TABLE OF CONTENTS

## LIST OF TABLES

## LIST OF FIGURES

## ABSTRACT

Linear systems work very well for the transmission of discrete-time continuous amplitude samples in poor signal-to-noise conditions, but their performance does not improve when the quality of the channel increases. Specifically, for high signal-to-noise ratios the gap with respect to the theoretical bounds is extremely large and, therefore, a more suitable method must be found. This is why non-linear encoding schemes have been studied, and several solutions have been proposed that outperform the classic linear approach.

In this thesis we present analog non-linear mappings with very simple and flexible design methods, low encoding and decoding complexity, and great robustness against noise. All these characteristics make them very versatile codes ready to be applied in many different scenarios. For example, successful results have been achieved in the transmission of images by creating an analog joint source-channel encoding scheme that combines Compressed Sensing measurements with our non-linear analog codes. We also show an extension of this communication system for underwater acoustic channels and non-linear channels.

# Chapter 1

# INTRODUCTION

## 1.1 Motivation

The raising of telecommunications during the last decades has profoundly revolutionized our society enabling the transmission of high rates of information not only through wired channels, but also wirelessly.

The extensive research done in this field has focused mainly in digital communication systems based on the separation of source coding and channel coding, since it has been proved that such architectures can reach theoretical optimal performance [39]. However, this result is only possible under the assumption of communication schemes with unrestricted complexity, meaning infinite processing and decoding capabilities. Although these systems are implemented in practice and they indeed perform really close to the theoretical limits, they still suffer from the aforementioned complexity problems, leading to significant delays due to the large blocks of information that need to be processed.

As complex communication scenarios such multisensor networks become common place, the need for new architectures that make an efficient use of the resources becomes crucial, because the autonomy of each terminal comes determined not only by the energy consumption at the transmission stage but also in the processing performed at the encoder and decoder.

As an answer to this demand, analog communication systems [18, 17, 19, 30] have arisen during the last years to try to reduce energy consumption. Surprisingly, some of these systems are based on the space filling curves presented more than fifty years ago by Shannon [40] and Kotel'nikov [31]. Inspired by their geometric point

of view of communications, time-discrete analog-amplitude non-linear mappings have been designed for some scenarios where the resulting performance is also very near to the theoretical bounds but with much less complexity than that of standard systems based on separation. Moreover, the non-linear nature of these codes allows them to outperform the classic linear approach in analog coding, where the system performance does not improve with increasing signal to noise ratios.

For all these reasons, we consider that this new field has a lot of room for growth. This thesis will have a stronger focus on maintaining the complexity of our proposed systems as low as possible.

## 1.2 Contributions

This thesis deals with low complexity non-linear analog mappings for the transmission of images in the AWGN channel and underwater channel. Among its main contributions we present the following ones:

- Low-complexity approximation of the 2:1 Archimedean spiral mapping avoiding numerical methods and drastically reducing the number of computations.
- Low-complexity 1:1 mapping for further performance improvement when transmitting images in channel conditions of low signal-to-noise ratio.
- Improved energy allocation for the transmission of compressed sensing measurements of an image.
- Extension of a full analog communication system for underwater channels avoiding intersymbol interference and achieving high information rates.
- Design of analog mappings for non-linear transducers used in underwater communications.

## 1.3 Organization

The remainder of this thesis is organized as follows: Chapter 2 contains some preliminary explanations on non-linear mappings and compressed sensing. Chapter 3 describes a full analog scheme where compressed sensing and low complexity non-linear mappings are combined to act as a joint source-channel encoder. Chapter 4 extends the previous architecture for a new scenario, i.e., underwater acoustic communications where, besides Gaussian noise, channel models are known to have very long tailed impulse responses. Chapter 5 depicts a new family of analog mappings for non-linear transducers often found in underwater acoustic communications. Finally, Chapter 6 presents our conclusions. The document ends with the bibliography.

# Chapter 2

# BACKGROUND ON NON-LINEAR MAPPINGS AND COMPRESSED SENSING

In this chapter we introduce a few basic concepts and give some preliminary comments on two topics that will be highly referenced throughout this thesis: space filling curves and compressive sensing. They both share the capability to operate in the analog domain with a non-discrete alphabet and have contributed to simplify in a great manner the complexity of signal acquisition and signal processing stages, as compared to the classical digital paradigm. One of the main reasons for this is that exploiting signal correlation becomes much easier in the analog domain (i.e. at the waveform level) than after quantizing the samples to a block of bits, where all that correlation is normally lost.

## 2.1 Non-linear Mappings

When transmitting discrete-time analog-amplitude samples over additive white Gaussian noise (AWGN) channels, there is a well-known theoretical limit [39] defined by $R_C R(D) < C$, where $R_C$ is the code rate, $R(D)$ is the rate-distortion function and $C$ is the channel capacity. Digital systems based on separating source coding and channel coding into two different blocks are able to reach optimal performance, but require the use of powerful vector quantization or channel codes, which may be problematic in practical applications due to the high encoding/decoding processing capabilities, large block lengths and severe delays that those techniques involve. Notice that the energy consumed at the transmission stage is not the only one determining the autonomy of a communication system. In that sense, it is equally important the often less mentioned energy consumption at the processing stage. As straightforward

as it seems, the simpler the encoding/decoding task is, the longer autonomy will be reached by our communication device. Moreover, systems with a design criterion based on separation lack flexibility and do not adapt gracefully to variations of the channel conditions (threshold effect). If the channel signal-to-noise (CSNR) ratio improves, the desired rate and distortion cannot be changed and the performance gets stuck. On the other hand, if the intensity of the noise increases, the system is forced to work under conditions it was not designed for and its performance experiences a drastic degradation.

Inspired by the fact that analog communications are optimal in some specific scenarios (such as transmission of Gaussian samples over a AWGN channel of the same rate) with very little complexity involved, many authors [18, 17, 19, 30] have investigated over the last years other schemes that "match" the number of source samples with the number of available channel uses and successfully leap over the traditional digital communications paradigm. The geometrical interpretation of communication systems and space filling curves proposed more than 50 years ago by Shannon [40] and Kotel'nikov [31], has renewed its relevance thanks to the coding schemes proposed by Fuldseth [15], Chung [8], Ramstad [36] and Hekland [22].

In order to describe the main idea of the space filling curves, let us take as a beginning example the Archimedean spiral shown in Figure 2.1. Notice that, as opposed to a line or a higher order polynomial function, a spiral fills the whole space as it grows and can approximate any point of the plane by projecting that point onto the spiral. This is precisely the key idea: given that the distance between every loop of the spiral is fixed, we could use just one parameter (the length or the angle of the curve) to represent with bounded distortion a point in the plane (i.e. two source samples).

Let us develop this concept by taking a look at its parametric equations [8, 22] (actually, these equations describe a 90º rotated version of the spiral shown in Figure

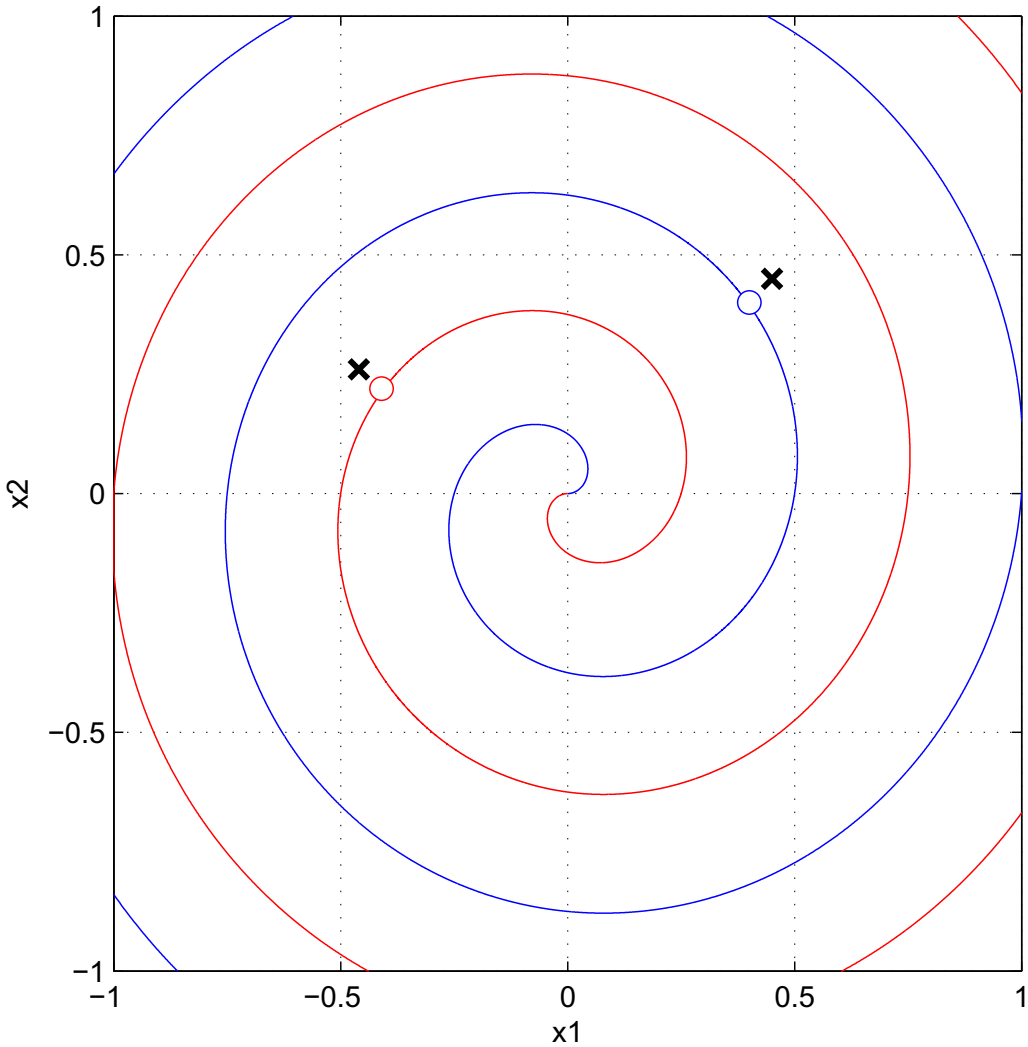


**Figure 2.1:** Two points in the plane and their closest neighbors belonging to the spiral.

2.1, but symmetry issues will not affect our analysis)

$$\begin{cases} x_1 = \text{sign}(\theta)\dfrac{\Delta}{\pi}\theta\sin\theta \\ x_2 = \dfrac{\Delta}{\pi}\theta\cos\theta \end{cases} \quad \text{for } \theta \in \mathbb{R}, \tag{2.1}$$

where each branch of the spiral corresponds to the positive or negative values of the angle $\theta$, and $\Delta$ is a positive scalar that determines the separation between each loop of the spiral. As mentioned above, it is important to realize that given that $\Delta$ is fixed, now we can represent any couple of source samples $X = \{x_1, x_2\}$ by its closest neighbor $\hat{\theta}$ belonging to the spiral. We will call this procedure mapping function $\hat{\theta} = M_\Delta(X)$, which depends only of $\Delta$. We will later discuss what is the criterion to choose the value of $\Delta$.

Now, generalizing this idea to higher dimensions, if we had an $N$ dimensional space where a space-filling surface of dimension $K$ lived ($N > K$), the encoder could approximate a tuple of $N$ source samples by simply projecting it onto the space-filling surface and getting its $K$ coordinates. Specifically, let $X = \{x_i\}_{i=1}^N$ be the source vector and $Y = \{y_i\}_{i=1}^K$ (or just $y$ when $K = 1$) be the coded vector containing the new coordinates in the subspace of the space filling curve. We can express this projection operation as a highly non-linear mapping function $M_{\text{NL}}()$ so that $Y = M_{\text{NL}}(X)$.

The decoder will obtain an estimate of $X$ from $Y$, that is, $\hat{X} = f(Y)$, where $f()$ is some decoding method. Notice that the coefficients in $Y$ might be corrupted with some noise which may lead to an interesting discussion on how to design $f()$.

- Maximum likelihood (ML) decoding:

  The ML estimate $\hat{X}_{\text{ML}}$ is calculated from a received symbol $Y$ as the source tuple belonging to the curve that satisfies:

$$\hat{X}_{\text{ML}} = \underset{X \in \text{curve}}{\text{argmax}}\{p(Y|X)\} \tag{2.2}$$

$$= \{X | X \in \text{curve and } M_{\text{NL}}(X) = Y\}. \tag{2.3}$$

This method has very low complexity and gives a fair estimation of $X$ with a few simple calculations. It performs very well for high CSNR and it is a decoding method that we will use extensively throughout this thesis.

- Minimum mean square error (MMSE) decoding:

  Much more powerful than ML, the MMSE decoding is optimal under a mean square error criterion. The estimated source tuple is given by

$$\hat{X}_{\text{MMSE}} = E\{X|Y\} = \int Xp(X|Y)\mathrm{d}X \tag{2.4}$$

$$= \frac{1}{p(Y)}\int Xp(Y|X)p(X)\mathrm{d}X. \tag{2.5}$$

  Notice that $p(Y|X)$ is highly non-linear and does not have a closed form, therefore, it can only be evaluated numerically. In [25] an interesting simplification is presented by discretizing $X$, $p(Y|X)$ and $p(X)$, and storing their value off-line, which drastically reduces the complexity of this decoding method.

Interestingly, it is possible to calculate the optimal performance theoretically attainable (OPTA) by the best encoder/decoder combination in a scenario that will be frequently used during this thesis: a source producing Gaussian samples with zero mean and $\sigma_S^2$ variance, the average power for transmitting a channel symbol limited to $\sigma_C^2$, and an AWGN channel with noise variance $\sigma_n^2$. By denoting as $\sigma_D^2 = \frac{1}{N}E\{\|X - \hat{X}\|^2\}$ the distortion we aim to minimize, and setting the rate distortion function equal to the capacity rate, it is easy to show that the OPTA is

$$\frac{\sigma_S^2}{\sigma_D^2} = \left(1 + \frac{\sigma_C^2}{\sigma_n^2}\right)^{K/N}, \tag{2.6}$$

where the term on the left is denoted as signal-to-distortion (SDR) ratio and is usually expressed in logarithmic form, i.e. SDR $= 10\log\frac{\sigma_S^2}{\sigma_D^2}$; and the second term inside the brackets is the linear form of the CSNR $= 10\log\frac{\sigma_C^2}{\sigma_n^2}$. It should be noted that this

bound is valid for both bandwidth compression ($N > K$) and bandwidth expansion ($N \leq K$).

We end this section by coming back to our previous scenario and letting $N = 2$ and $K = 1$ so that we can compare how well does the $2:1$ Archimedean spiral perform against the theoretical limits. First, we had a pending discussion regarding $\Delta$ that will be better understood now that we have introduced our communication framework. Note that for very small values of $\Delta$, the loops of the spiral will grow very close from each other and thus we will be able to represent with very little distortion any source sample standing in the middle of the two arms. On the contrary, the more loops we need to describe a point in the plane the less protection against noise we will have, and we will be using more energy in our channel symbols. Therefore, this trade-off needs to be solved according to the amount of power available in each scenario.

Second, we need to define an invertible function often found in the literature which is just an exponential transformation

$$T_\alpha(x) = \text{sign}(x)|x|^\alpha \quad \text{for } x \in \mathbb{R} \text{ and } \alpha \in (0, 2]. \tag{2.7}$$

This 1:1 non-linear mapping is usually placed after the Archimedean spiral encoder and it is used to alter the energy distribution of the channel symbols. The most typical value is $\alpha = 2$ [8, 22], because it leads to very good performance in most situations and also enables theoretical analysis, as compared to non integer values. However, it was shown in [25] that optimizing its value for every CSNR improves performance significantly, particularly when working at the low CSNR regime and decoding with ML criterion.

The simulated setup is described in Figure 2.2. The source vector samples $X$ are projected into the spiral and next, the non-linear transformation $T_\alpha(\cdot)$ is used. After an energy normalization stage, channel symbols get corrupted by the AWGN process

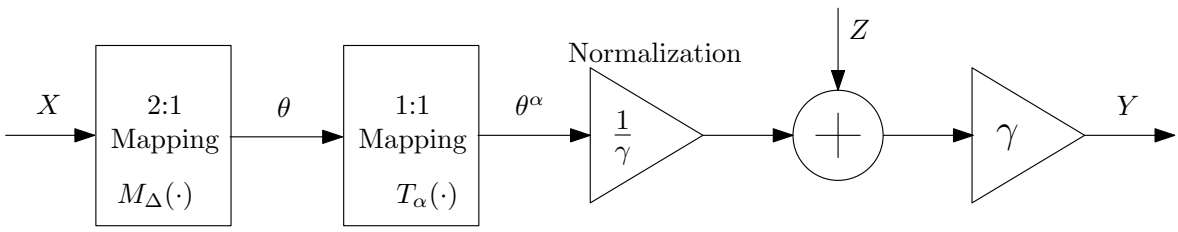


**Figure 2.2:** Simulated 2:1 framework based on non-linear mappings

$Z$ and, finally, the received symbols $Y$ are decoded. Expressed mathematically,

$$Y = T_\alpha(M_\Delta(X)) + \gamma Z. \tag{2.8}$$

As for the decoding, both ML and MMSE are considered following the same strategy as in [25], where the optimum value of $\Delta$ and $\alpha$ will be used for each decoding method and each CSNR value.

To illustrate the concepts introduced in this chapter, Figure 2.3 presents the performance of ML and MMSE decoding when the mapping described above is used for the transmission of Gaussian sources over AWGN channels. The parameters $\Delta$ and $\alpha$ are optimized for each CSNR. For comparison purposes, the OPTA for 2:1 systems as well as the OPTA for linear mappings is also included. First of all, it should be noted that the OPTA and the linear OPTA start very close from each other, but as the CSNR increases they drastically diverge. Thus, it is very clear that in order approach the theoretical bounds, we need to investigate other alternatives to linear systems. That is exactly where our mappings come into play and show their outstanding potential by performing closer than 2 dB for all the CSNR range. In particular for high CSNR, this difference is reduced to just 1 dB even for a simple strategy such as ML detection. Notice that the more complex procedure of MMSE decoding clearly overperforms ML decoding for the whole CSNR range, specially in the low CSNR range, where it even beats the linear OPTA bound and stands really close to the theoretically reachable limits.

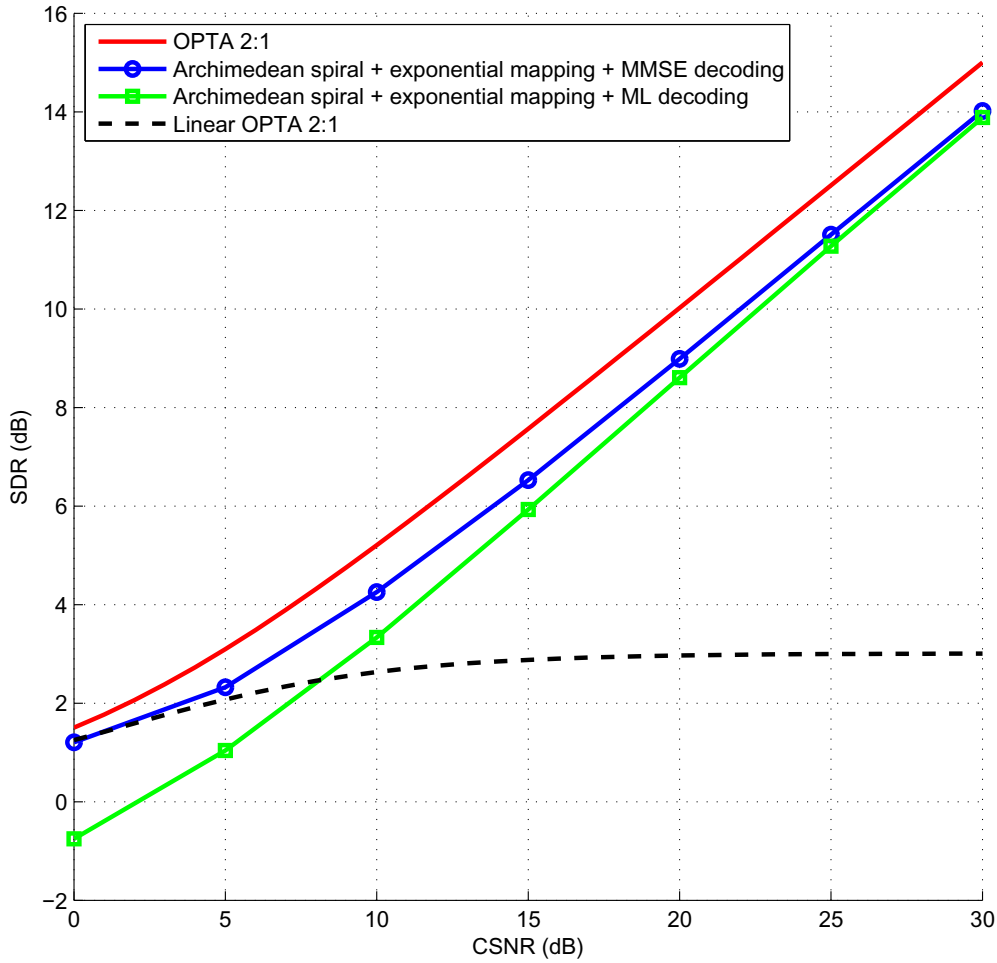


**Figure 2.3:** Performance of ML and MMSE decoding for the transmission of Gaussian sources over AWGN channels using the mapping described in the text. The theoretical limits are also provided.

## 2.2 Compressed Sensing

A key to the success of compressed sensing [1, 4, 5, 6, 10] is its capability to reconstruct the original signal from a limited number of measurements at sub-Nyquist sampling rates. The Nyquist sampling theorem, which is one of the most important foundations of digital signal processing, considers only the frequency support of the signal, not its actual information content. Therefore, it often occurs that for broadband signals it is very hard to implement systems with a hardware that can reach the minimum Nyquist rate, due to the sampling speed and acquisition windows that are required. Another problem is that the resulting samples might well be correlated so that a source encoder will be needed to significantly reduce the amount of processed and transmitted samples.

Interestingly, the classical digital approach of sampling and quantizing can be leaped over by compressed sensing. The only assumption is that the original signal $\underline{x} \in \mathcal{R}^N$ admits a $T$ sparse representation in some basis $\Psi = [\underline{\psi}_1, \underline{\psi}_2, \ldots, \underline{\psi}_N]$, meaning that $\underline{x} = \Psi\underline{\beta}$ where $\beta$ is an $N \times 1$ vector with only $T$ nonzero entries. If this occurs, then we will be able to reconstruct the original signal from $M$ measurements, with $M = O(T \log N)$ and $M \ll N$. This allows to relax the acquisition requirements and reduce the complexity of the sampling process, as compared to the more restrictive conditions that Nyquist theorem dictates.

The way those $M$ measurements are obtained is by performing linear projections of $\underline{x}$ with a random matrix $P$ of size $M \times N$. Let $\underline{y}$ be the $M \times 1$ vector storing the measurements, then we can express our acquisition method as $\underline{y} = P\underline{x}$. In order to guarantee a successful recovery of $\underline{x}$ from $\underline{y}$ with high probability, each row of $P$, $\phi_i$, must be incoherent with the columns of $\Psi$, $\psi_j$. The coherence between those two bases is defined as: $v(\Psi, P) = \sup\{|\langle\psi, \phi\rangle| : \psi \in \Psi, \phi \in P\}$, and it is known that many pair of bases $(\Psi, P)$ can be found satisfying the low coherence property.

As for the reconstruction of $\underline{x}$ from $\underline{y}$, we can take a realistic approach and consider that some noise is present and our measurements will be corrupted: $\underline{y}_n = \underline{y} + \underline{n}$ where $\underline{n}$ is a zero-mean additive white Gaussian noise. An estimation of the original

signal $\underline{\hat{x}} = \Psi\underline{\hat{\beta}}$ can be constructed by using the Basis Pursuit Denoising [7] algorithm that solves the following minimization problem: $\underline{\hat{\beta}} = \arg_{\underline{\beta}} \min \|P\Psi\underline{\beta} - \underline{y}_n\|_2^2 + \lambda\|\underline{\beta}\|_1$ subject to $\underline{y}_n = P\Psi\underline{\beta} + \underline{n}$, where the value of $\lambda > 0$ is given by the amount of channel noise.

Since $\underline{x}$ is given, the critical parameter of design is the measurement ensemble $P$. If hardware issues are to be considered, not only it needs to have a dense representation in the sparsity basis $\Psi$, but it also needs to be generated in a computationally efficient manner, it must be easy to store in memory, and, finally, it should enable fast algorithms for reconstruction.

Extensive work has been done in this field and measurement matrices of very different nature have been proposed for this matter. For example, matrices where each element is an i.i.d. Gaussian sample or follows a Bernoulli distribution. However, taking into account as an example the dimensions of a high definition picture, the huge amount of storage required by these methods makes them unfeasible for practical applications. On the other hand, more sophisticated methods propose incoherent sampling in a transform domain as a way to get matrix $P$. A big advantage for these methods is that the transform domain can be equipped with fast transform algorithms which enable rapid computations. Some examples of measurement ensembles achieving good performance are partial Fourier ensemble, scrambled Fourier ensemble, scrambled block Hadamard ensemble and noiselets [3, 4, 16].

Nevertheless, all these sampling approaches fail to exploit any previous knowledge of the original signal other that its sparsity. Recently, some authors [12, 13, 41] have started to use *a priori* information to achieve improved performance. Throughout this thesis we will be using the method presented in [46], where the designed measurement ensembles efficiently exploit the statistical distribution of natural images in the sparse wavelet domain.

Natural 2D images do not usually exhibit great discontinuities, on the contrary, they usually have big monochromatic areas with smooth transitions and almost no change from pixel to pixel. Hence, the image will be mostly represented by coarse

scale wavelets with their spectral energy in the Fourier domain clustered over the low frequency band. It is also known that in natural images the magnitude of wavelet coefficients decrease exponentially from coarse scales to fine scales [37]. Based on this probability function, a random sampling strategy may select wavelet coefficients with exponentially decaying probability as they correspond to higher frequencies. This will result in variable density sampling patterns, as shown in Fig. 2.4, where samples will be kept with higher probability if they correspond to low frequency subbands. This method does not require image dependent information and is flexible enough to adapt to different decaying rates and desired number of measurements. Analogously, a variable density probability function can be defined for the Discrete Hadamard Transform. This technique has been applied successfully in [46] and we will use it in this thesis.

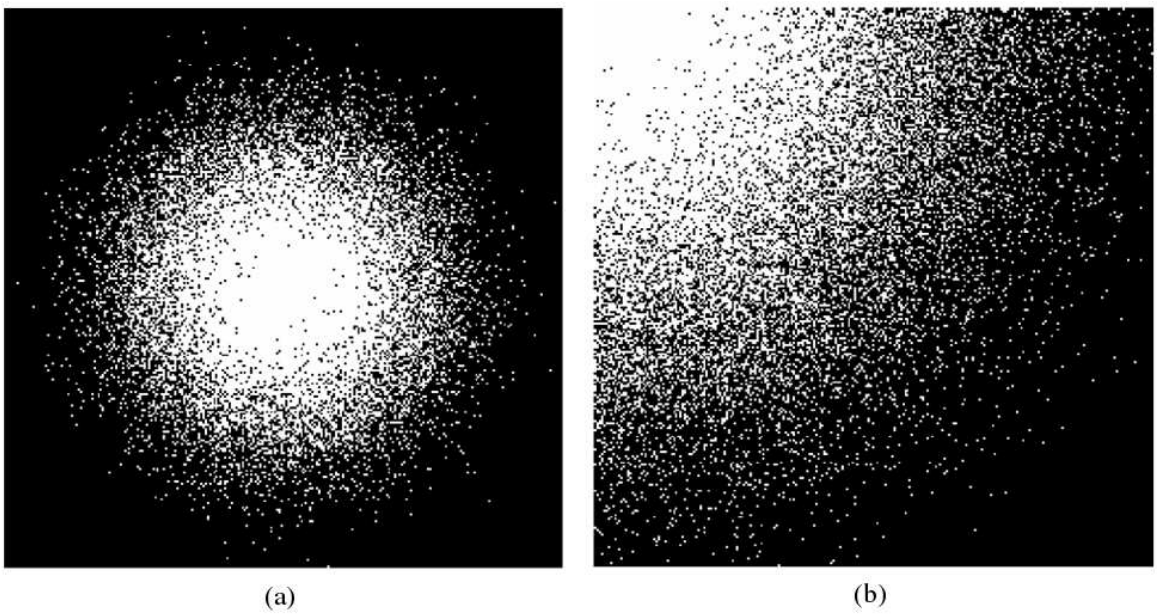


**Figure 2.4:** Variable density sampling patterns for (a) DFT domain (b) DHT domain.

# Chapter 3

# NON-LINEAR MAPPINGS FOR THE TRANSMISSION OF COMPRESSED SENSING IMAGES

In this chapter we propose a communication-system designed for the transmission of images over AWGN channels by combining compressed sensing and analog non-linear mappings. The proposed scheme acts as an analog joint source-channel encoder where bits are never utilized. The time-discrete analog-amplitude samples produced by the source are processed by the compressed sensing encoder and, next, further compressed by our analog non-linear mapping producing continuous amplitude symbols that will be sent directly through the noisy channel. A new 2:1 mapping is presented whose complexity is almost negligible and energy allocation improvements are also discussed. Simulation results for our proposed framework outperform in a significant way the stand-alone compressed sensing system for the whole signal-to-noise range.

## 3.1 Introduction

It is well-known that digital systems based on separation of source and channel coding are theoretically optimal under the assumptions of very long input data vectors and high complexity at the encoding/decoding blocks [39]. Since these are strong assumptions, the price to pay for real systems with near capacity performance is severe delays and the need of huge data processing capabilities (which may lead to less autonomy in energy-critical scenarios). In addition, non-adaptive digital systems do not show a good behavior when working outside the CSNR they were designed for: if the channel conditions improve, they overprotect the channel symbols and the end-to-end

performance does not improve. On the other hand, if the channel noise increases, the whole system crashes.

In this chapter we present a full analog framework for transmitting images through AWGN channels, where bits are never utilized and aiming at alleviating the problems that traditional digital systems suffer from. The main idea is to build our communication system out of the concatenation of two blocks: a compressive sensing [1, 4, 5, 6, 10] encoder and non-linear mappings [31, 40, 25], so that the time-discrete analog-amplitude CS measurements are further compressed by the non-linear mappings producing analog channel symbols that will be sent directly through the AWGN channel. Thus we can see the proposed system as a full analog system where an analog source encoder (the CS block) is followed by an analog joint source-channel encoder (the non-linear mapping).

The remainder of this chapter is organized as follows. In Section 3.2 we review the proposed discrete-time all-analog-processing communications system. We also propose two very low complexity non-linear mappings and explain the proposed energy allocation method. Section 3.6 presents the simulation results. Conclusions are provided in Section 3.7.

## 3.2 Proposed System

Figure 3.1(a) shows a communication system based on stand-alone CS. The $M$ measurements obtained at the output of the CS block are directly used as the channel symbols without any further processing. On the other hand, our proposed scheme shown in Figure 3.1(b), makes use of space filling curves and energy allocation. First, the CS block acts as a source encoder and reduces all the samples that define the image to just $1+k(M-1)$ measurements. Second, since the energy of those measurements is roughly exponentially decreasing, we make a simple band partition by separating the first symbol from the rest and allocating for it the proper amount of energy. The other $k(M-1)$ samples are processed by our $k:1$ analog non-linear mapping that works as a joint source-channel encoder, thus obtaining $M-1$ channel symbols. Notice that $k$

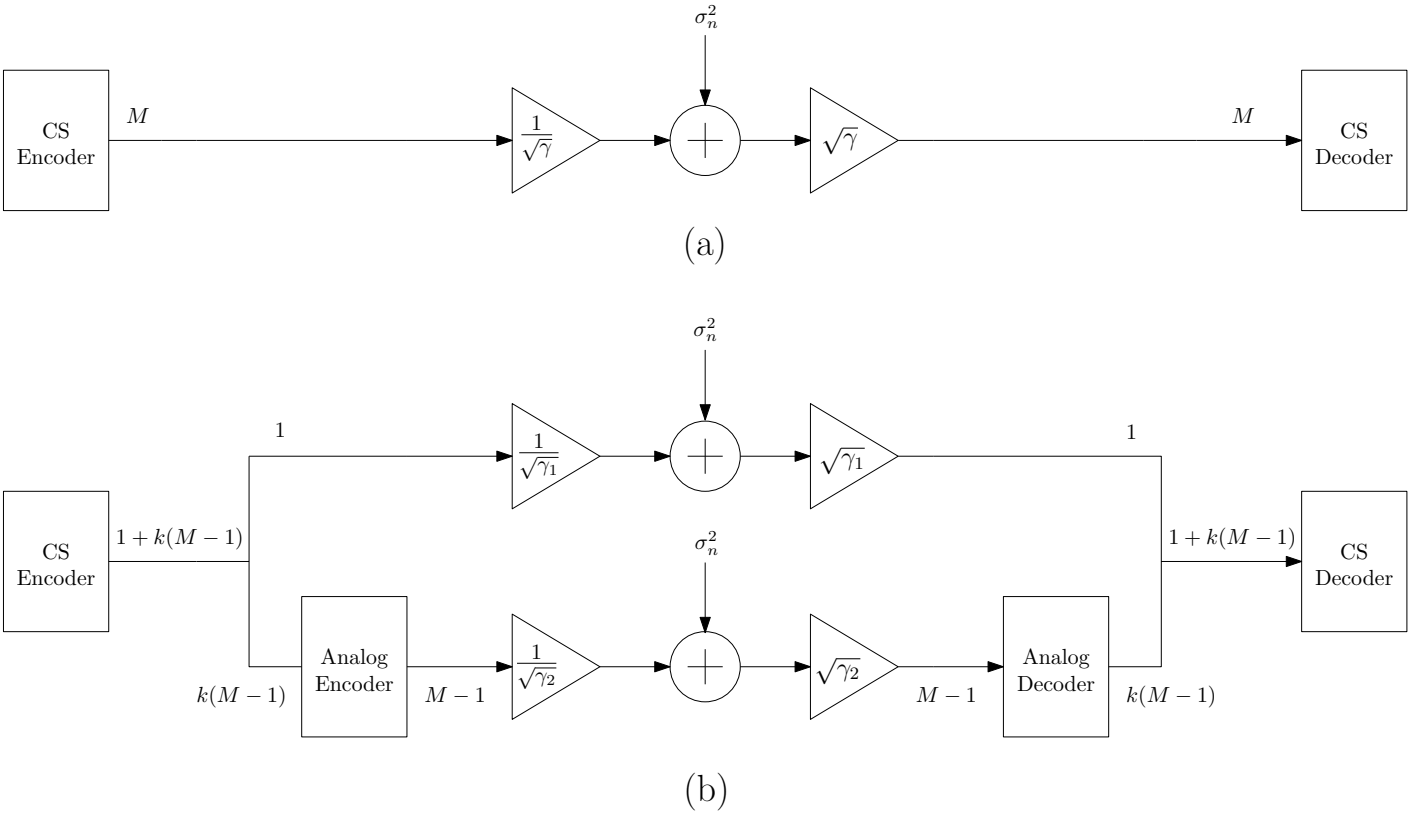


**Figure 3.1:** (a) Stand-alone compressed sensing system. (b) Proposed scheme.

gives us the system's compression ratio, and that its optimum value will need to be chosen according to the CSNR region we work at. Finally, it is important to realize that both (a) and (b) schemes use the channel the same amount of times: $M$.

In our proposed system, we will use three different space filling curves for transmitting the CS coefficients. The first one is a $4:1$ bandwith compression spiral-like

curve [14].

$$\begin{cases} x_1 = \text{sign}(\theta)\dfrac{\Delta}{\pi}\theta \sin\dfrac{\theta}{3\pi}\cos\theta \\ x_2 = \text{sign}(\theta)\dfrac{\Delta}{\pi}\theta \cos\dfrac{\theta}{2\pi}\sin\theta \\ x_3 = \dfrac{\Delta}{\pi}\theta \sin\dfrac{\theta}{2\pi}\sin\theta \\ x_4 = \dfrac{\Delta}{\pi}\theta \cos\dfrac{\theta}{3\pi}\cos\theta \end{cases} \quad \text{for } \theta \in \mathbb{R} \tag{3.1}$$

The second one is the non-linear mapping already presented in our previous chapter, i.e., the 2 : 1 bandwith compression Archimedean spiral. Its parametric equations [8, 22] are

$$\begin{cases} x_1 = \text{sign}(\theta)\dfrac{\Delta}{\pi}\theta \sin\theta \\ x_2 = \dfrac{\Delta}{\pi}\theta \cos\theta \end{cases} \quad \text{for } \theta \in \mathbb{R}. \tag{3.2}$$

The third non-linear mapping is the 1:1 exponential transformation, also defined in Chapter 2

$$T_\alpha(x) = \text{sign}(x)|x|^\alpha \ \text{ for } x \in \mathbb{R} \text{ and } \alpha \in (0, 2]. \tag{3.3}$$

As explained in the previous chapter, mappings (3.1) or (3.2) will be concatenated with the non-linear transformation (3.3), and the parameters $\Delta$ and $\alpha$ will be optimized for each CSNR. Notice that the channel symbols are normalized using a factor $\sqrt{\gamma}$ so that the average energy per transmitted sample is equal to 1; therefore obtaining a CSNR $= 10\log\frac{1}{\sigma_n^2}$, with $\sigma_n^2$ being the noise variance of our AWGN channel. In order to keep the system's complexity as low as possible, we will perform ML decoding at the receiver.

## 3.3 Circular Approximation

The encoding process for 2:1 systems described in the previous section can be simplified further, since projecting a tuple into the spiral involves solving non-linear

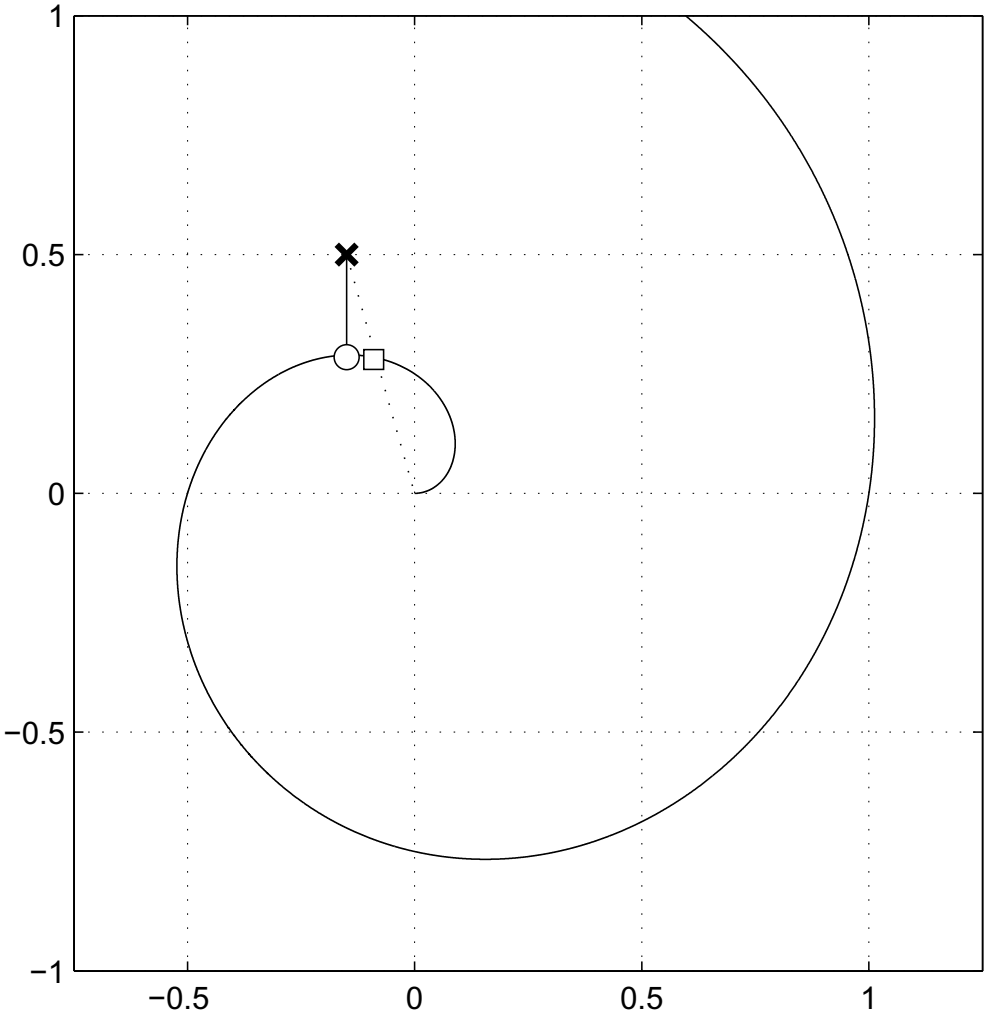


**Figure 3.2:** Circular approximation to the spiral curve. The exact mapping of the given source sample is given by the circle. Instead, we take a radial approximation and use the square.

equations through numerical methods. Hence, instead of projecting the point over the spiral, we will use the circular approximation shown in Fig. 3.2.

This approximation is based on the angular coordinate of the source sample. Notice from Fig. 3.3, that given a source sample $X$ with polar coordinates $(r, \varphi)$, there

are infinite points $\theta_i$ belonging to the spiral with the same angle $\varphi$ with respect to the origin. Each of these points is $\theta_i = \varphi + 2\pi i$ with $i = 0, 1, 2...$ and it is easy to show that the closest one to $X$ has the following index

$$i = \text{round}\left(\frac{r\pi - \varphi\Delta}{2\pi\Delta}\right). \tag{3.4}$$

It is obvious that the complexity of this calculation is almost negligible, thus making our circular approximation an interesting alternative to the exact projection based on numerical methods. Moreover, the farther the source point is from the origin, the more accurate our approximation will be.

Finally, in order to complete the description of our approximation one more comment is necessary. For the tuples close to the origin, we utilize the simple mapping shown in Fig. 3.4. We are now using an auxiliar semi-circumference that approximates the spiral near the origin, so that instead of projecting the source tuple into the spiral (which would give us the white circle symbol in the figure), we first project it into the semi-circumference, obtaining the diamond symbol. Then, we calculate the angle $\hat{\theta}$ of the diamond with respect to the origin, and plug the obtained $\hat{\theta}$ in (3.2) to get the square point as a result. Notice that if we had not used the auxiliar semi-circumference projection, but just the angle between the source pair and the origin, the mapped point (black square in the figure) would have been far away from the desired projection (white circle point), which would have led to a large distortion.

### 3.4 Complexity Results

In order to assess the simplicity of the proposed approximation, we now compare the average number of computations required to encode and decode a pair of source symbols using the standard 2:1 mapping given by (3.2) and the circular approximation. Because of their lower complexity, additions and products by a constant can be disregarded in general, but the figures in brackets show the total if they are counted.

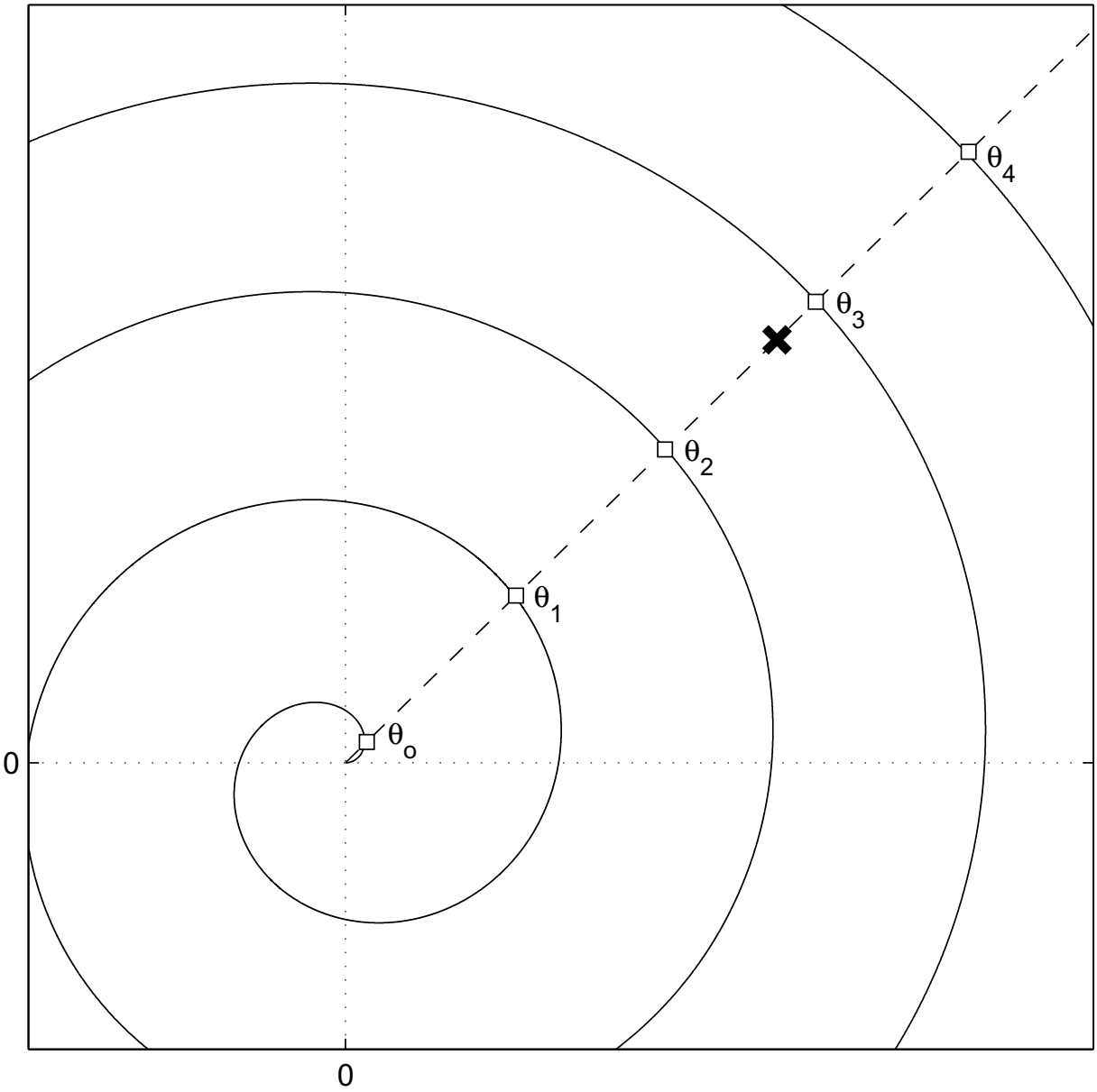


**Figure 3.3:** A source sample and all the points belonging to the spiral that share the same angle with respect to the origin.

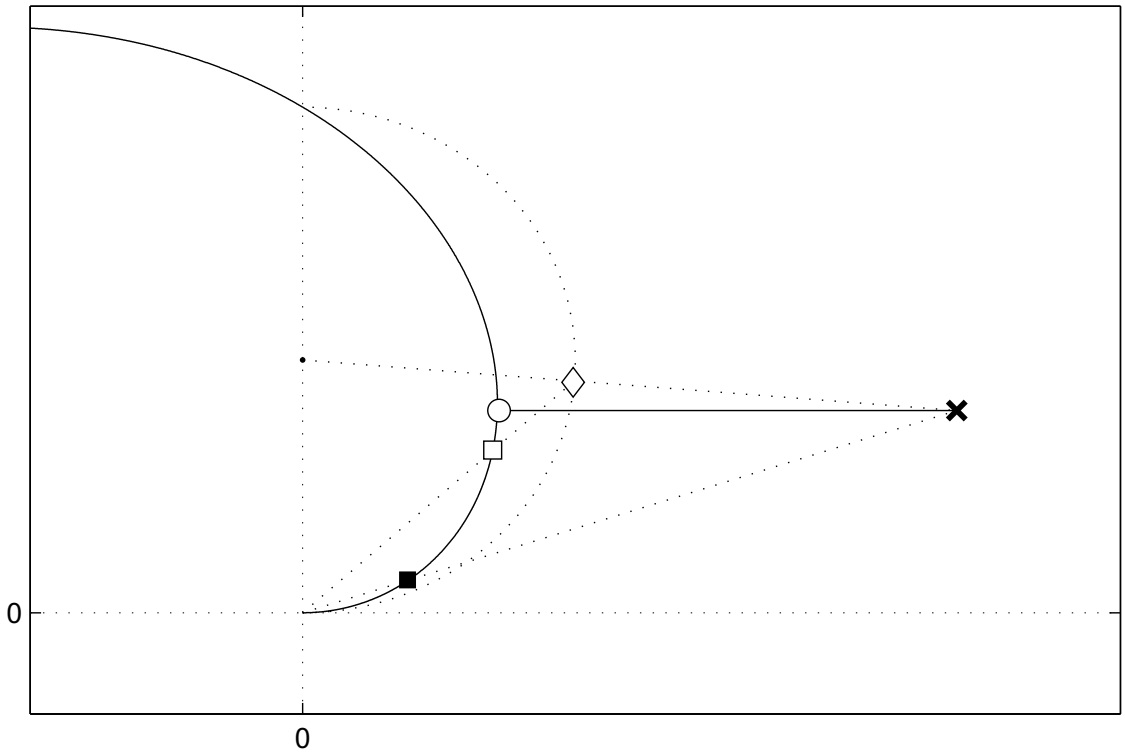


**Figure 3.4:** Circular approximation to the spiral curve in the region close to the origin.

| | Standard 2:1 map | Simplified 2:1 map |
|---|---|---|
| Products | 472 (764) | 4 (8) |
| Additions | 235 (294) | 3 (4) |
| Comparisons | 74 | 6 |
| Table look ups | 119 | 4 |

**Table 3.1:** Computations to encode a pair of source symbols.

| | Standard 2:1 map | Simplified 2:1 map |
|---|---|---|
| Products | 5 (7) | 5 (7) |
| Additions | 0 (2) | 0 (2) |
| Comparisons | 1 | 1 |
| Table look ups | 3 | 3 |

**Table 3.2:** Computations to decode a pair of source symbols when ML decoding is used.

As illustrated in Tables I and II, the number of computations using the circular approximation is dramatically reduced with respect to the standard mapping, so that the encoding process is two orders of magnitude faster, while the decoding complexity is extremely low in both cases. It would be impossible to find a digital system with similar performance and complexity.

### 3.5 Band Partition

The energy of the measurements proceeding from the CS block is not uniformly distributed. Thus, it is reasonable to divide them measurements into different energy bands and find the optimum parameters $\alpha$ and $\Delta$ for each band, as well as the optimal energy allocation for channel transmission. Obviously, an increase in the number of bands should lead to performance improvements, but we have observed that the biggest improvement appears when switching from one band to two bands. After that, the performance improves moderately. Thus, for the sake of simplicity, we will focus in the two-band case.

The first band consists of just the first symbol, which is sent uncoded through the channel, while the second band consists of the rest of the symbols, which go through the analog encoder and are sent over the noisy channel. In order to find the best performance we just need to find the optimum energy allocation for each band keeping in mind that the previous constraint of average energy per sample equal to 1 must be satisfied. Since the number of transmitted symbols (and thus the total energy) is $M$, this is equivalent to finding the best trade-off value $\rho$ (with $0 < \rho < 1$) between the

energy allocated to the first band $\rho M$ and the energy allocated to the second band $(1-\rho)M$. Note that the value of $\rho$ defines the scaling factors $\gamma_1$ and $\gamma_2$.

### 3.6 Simulation Results

We now show the performance of our system when transmitting five well-known pictures: "Baboon", "Boat", "Goldhill", "Lenna" and "Pentagon" (the same ones used in [46] for the sake of comparison).

Let us recall that our CS block takes $1 + k(M-1)$ measurements from each picture and that while the first CS symbol is sent uncoded, the rest are processed using our $k:1$ mappings. This way, the total number of transmitted symbols is $M$ and we will be able to compare our system with the CS stand-alone framework. In our particular case, we have used $256 \times 256$ grayscale images, with $M = 5000$ and three different values for $k$ ($k = 1, k = 2$ and $k = 4$). For the three cases we will optimize the energy allocation and at the decoder we will perform ML and apply the CS reconstruction algorithm.

Notice that for the $k = 1$ case there are two parameters ($\alpha$ and $\rho$) that need to be optimized for every CSNR, while for the $k = 2$ and $k = 4$ cases are three ($\alpha$, $\Delta$ and $\rho$). However, this task can be done once offline and store their optimum values in order to use them when necessary.

In Fig. 3.5 we show the optimal performance results obtained with the different approaches by plotting the SDR of the reconstructed image versus the CSNR. The first thing we can see is that the CS stand-alone approach shows poor performance in the low CSNR regime, and that this is greatly improved by introducing our 1:1 mapping with energy allocation. Still, both curves achieve their maximum value around CSNR=40 dB and get stuck beyond there no matter how much the channel improves. In order to improve performance for higher CSNR, $k > 1$ mappings must be used. For $k = 2$ both curves are able to increase the SDR by 2 dB and still show a good performance at the lower CSNR range of values. Also, notice how the standard 2:1 mapping and the one with the circular approximation pretty much overlap with each other, even though the

latter has negligible complexity as shown in Section 3.4. For $k = 4$, the performance increases slowly but steadily with the CSNR and at high CSNR it achieves the highest SDR value of all five curves thanks to its greatest compression rate.

Since these results are the average of five pictures, we show the individual results for each image. Figure 3.6 depicts those curves for the case of 2:1 circular approximation (for the other values of $k$ the results are equivalent). As expected, the performance is highly correlated with the amount of information of the image. Figures 3.7 and 3.8 show some reconstructions for the best and worst case scenarios, which happen to be "Pentagon" and "Baboon", respectively.

## 3.7 Conclusion

We have proposed a discrete-time analog-amplitude system for image transmission based on the combination of compressive sensing, non-linear mappings and energy allocation. The proposed framework can be considered as a full analog joint source-channel encoder with a strong focus in keeping a very low complexity. The new mappings presented show very interesting features such as speed and low complexity without compromising performance. Simulation results prove that they present significant improvement over previously proposed systems and the stand-alone CS framework.

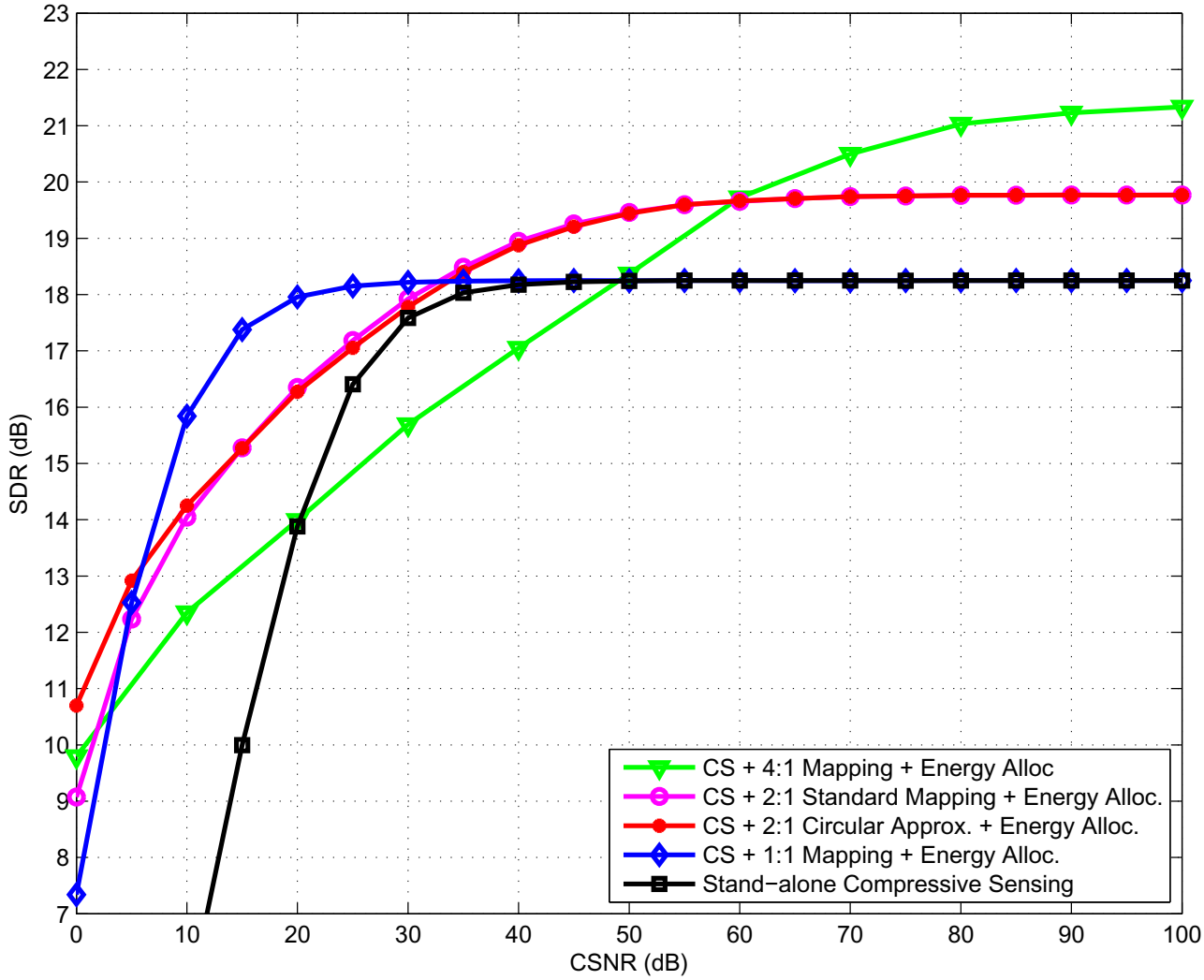


**Figure 3.5:** Average SDR of five reconstructed $256 \times 256$ gray-scale images versus the channel signal-to-noise ratio of an AWGN channel, with $M = 5000$ transmitted samples and ML decoding. For high CSNR the proposed system with $k = 4$ and $k = 2$ clearly outperforms the standard CS scheme ($k = 1$).

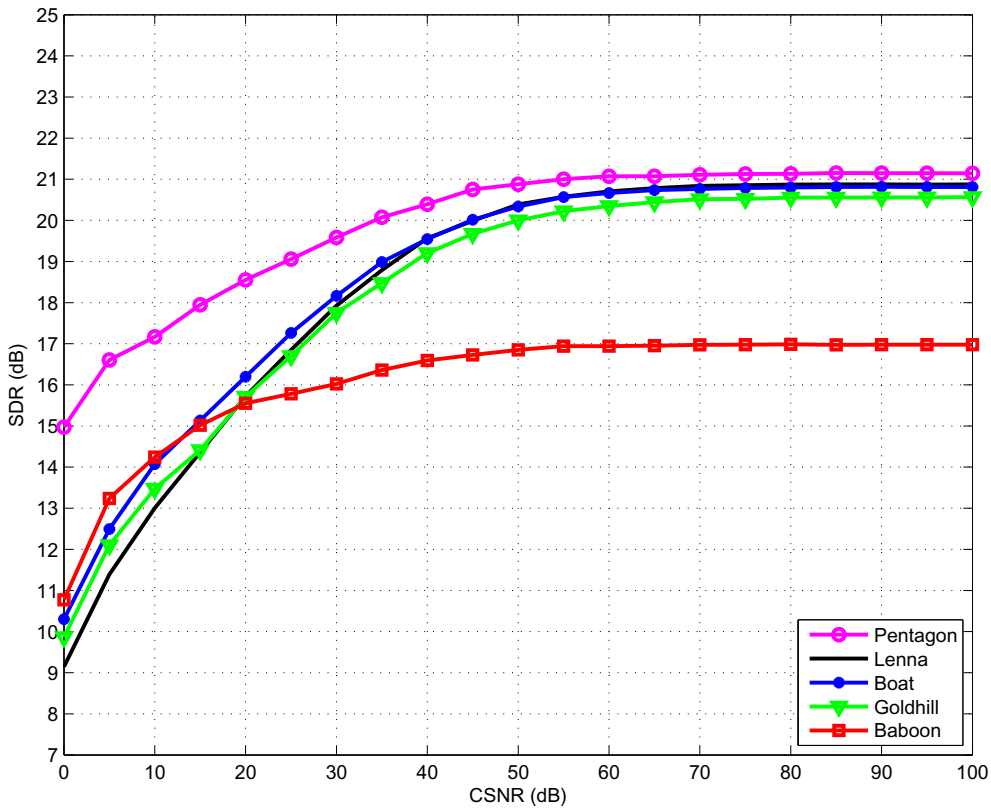


**Figure 3.6:** Individual SDR of five reconstructed $256 \times 256$ gray-scale images versus the channel signal-to-noise ratio of an AWGN channel, with $M = 5000$ transmitted samples, 2:1 circular approximation mapping and ML decoding.

(a) Original image.

(b) $k$=1; CSNR=20 dB; SDR=19.44 dB.

(c) $k$=2; CSNR=50 dB; SDR=20.88 dB.

(d) $k$=4; CSNR=90 dB; SDR=22.51 dB.

**Figure 3.7:** Reconstructions for "Pentagon".

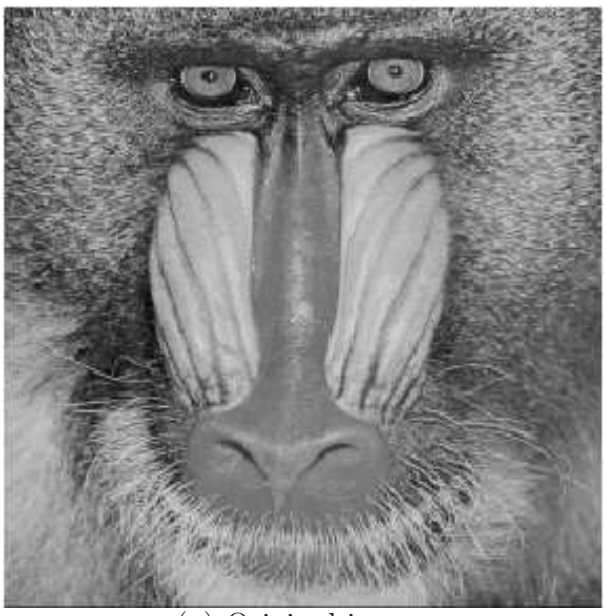

(a) Original image.

(b)$k$=1; CSNR=20 dB; SDR=16.02 dB.

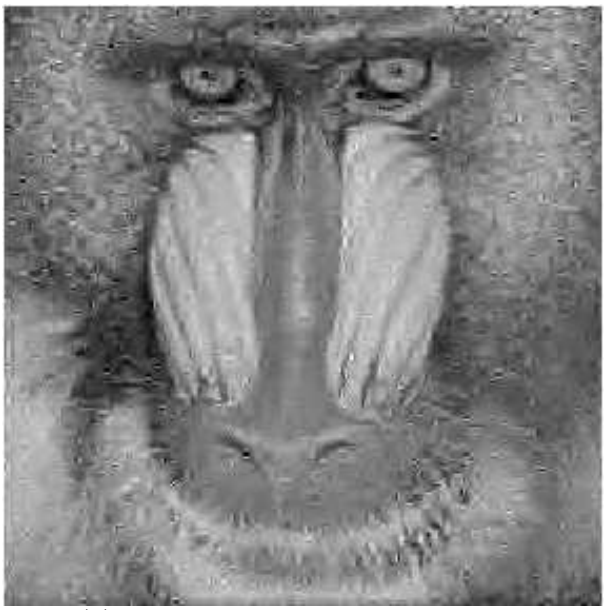

(c)$k$=2; CSNR=50 dB; SDR=16.85 dB.

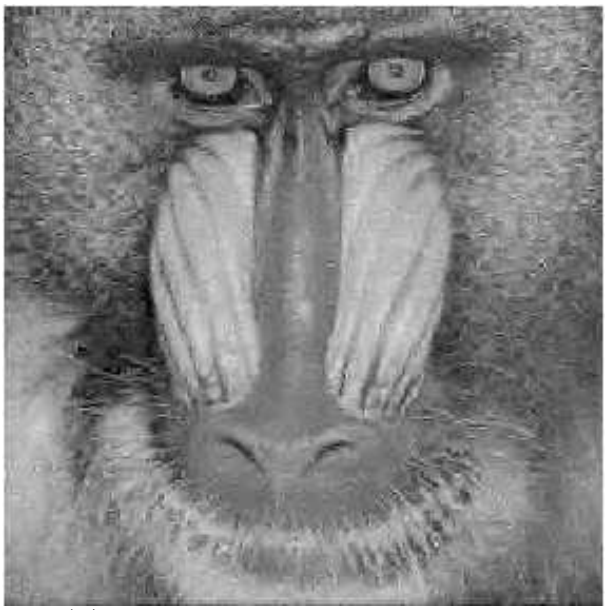

(d) $k$=4; CSNR=90 dB; SDR=17.73 dB.

**Figure 3.8:** Reconstructions of "Baboon".

# Chapter 4

# IMAGE TRANSMISSION OVER THE UNDERWATER ACOUSTIC CHANNEL

Over the last decades, a large number of improvements in the field of communications have made possible to develop systems capable of sending and receiving information at very high data rates. However, the underwater channel still remains as a very problematic case, due to its multipath spreading nature which produces intersymbol interference (ISI). This becomes a big constraint for achievable communication rates and, therefore, for high speed image transmission. Extending our previously presented framework, we propose a communication system for images where, again, bits are never utilized and we work only in the discrete-time analog-amplitude domain. We first acquire a reduced number of measurements through CS, further compress them using analog non-linear mappings, perform energy allocation adequately and send those symbols through the underwater channel. In order to minimize the disortion effects caused by the ISI, at the receiver we perform the conventional MMSE equalization process. Simulations using channel models derived from overseas experiments show that image transmission is reliable using our proposed method.

## 4.1 Introduction

Underwater communications are becoming more and more important with the increasing relevance of applications such as undersea disaster response or undersea rescue. Also, many other disciplines such as ocean monitoring could greatly benefit from new underwater communication systems if their rates where comparable to the ones achieved in AWGN channels. Nevertheless, electromagnetic waves suffer from great attenuation under the sea, so acoustic waves are often used as information carriers [29],

despite their narrow bandwidth (around 30 kHz in distances of 1-10 km). The biggest problem, however, is the multipath spread that produces very heavy-tailed impulse channel responses that cause severe intersymbol interference (ISI) for all communication setups.

Over the last decades, many digital communication systems [45], [44] have tried to overcome all these problems, usually achieving rates of several tens of kbps. Direct transmission of digital images has been tried [9] and 48 kbps rate achieving frameworks have been presented [38] combining heavy processing strategies such as MIMO architecture, turbo codes and space-trellis codes. Therefore, there is still a great need of low-complexity high-speed communication systems that will enable the next generation of ocean missions.

## 4.2 Proposed System

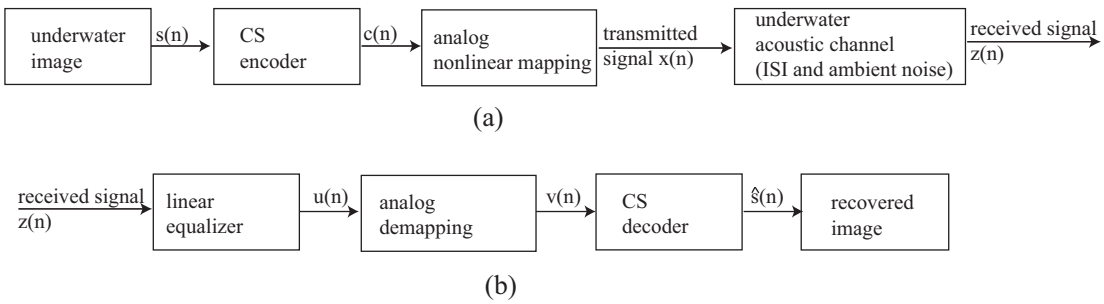


**Figure 4.1:** Proposed system: (a) Signal adquisition and encoding. (b) Signal decoding and image reconstruction.

Our proposed system consists of a combination of CS, non-linear mappings and energy allocation, as well as a a linear equalization stage in order to avoid as much as possible the ISI effects of the underwater channel. Again, bits are never utilized and we operate the whole time in the discrete-time analog-amplitude domain.

Figure 4.1 shows the block diagram of our communication system where, using CS, we first obtain in an efficient manner a reduced set of measurements corresponding to our underwater image. This acquisition method works as an analog source encoder

since it drastically reduces the amount of symbols that need to be processed and sent through the channel. We later use our analog non-linear mappings that will protect the symbols from the channel distortion, and depending on the case, further compress the symbols too. Thus, we can consider this block as a joint source-channel encoder. Next, after reassigning the proper energy to our channel symbols, we will modulate them to the carrier frequency so that they can be sent through the acoustic channel. Due to its multipath nature, our symbols will be corrupted not only with noise but also with ISI, so we have included a linear MMSE equalizing module in our receiver. Following the equalization stage, an analog demapper can be found which will decode our symbols under a maximum-likelihood criteria. The interesting part about this decoding structure is that it has negligible complexity without compromising performance. Finally, the CS decoder rebuilds the original image.

We will now complete this description with some technical details. However, since the CS block, the non-linear mappings and the energy allocation method were already described in Sections 2.2, 3.3 and 3.5. respectively, rather than covering those topics again, we will discuss the integration between the first two blocks and, next focus on the ISI part, which is the main characteristic of the underwater channel.

### 4.2.1 Integration of CS with Non-linear Mappings

While the CS part remains untouched in this chapter, we do not use the $4:1$ mapping (Equation 3.1) for two reasons. The first one is that its maximum performance appears at very high CSNR values, which are not representative of usual underwater communication systems. The second one is that compared to 1:1 and 2:1 mappings, it is the one with the highest complexity.

We define as "system rate" the total compression ratio achieved by the CS block and the analog mappings together. For example, if the source generates $L$ samples and we can only transmit $L/4$ symbols, the system rate must be 4:1. The open question now is whether it is best to have a 2:1 CS rate and a 2:1 spiral mapping, or instead, use a 4:1 CS compression ratio and a 1:1 non-linear mapping. This is closely related to

the classical problem when designing a communication system. Is it better to transmit more information per symbol and less protection against noise, or send less information but adding more redundancy?

In our case, looking at the results in the previous chapter and in [26], we can say that at low CSNR values the best option is to use 4:1 compression at the CS stage followed by a 1:1 mapping. On the other hand, in the high CSNR regime, we should compress also at the mapping stage and thus we use a 2:1 rate in both blocks. This makes sense since CS techniques are similar in many ways to linear codes, and we know from [32] that their perfomance gets stuck at high CSNR. We will confirm these ideas later in our simulations.

### 4.2.2 Dealing with ISI

The multipath phenomenon existing in underwater communications makes symbols sent at different time slots arrive together at the receiver and severely corrupt our signal. Taking this channel model into account, we can go back to Figure 4.1 and let our received signal be $z(n) = x(n) * h(n) + w(n)$; where $x(n)$ is the stream of transmitted symbols, $h(n)$ is the channel impulse response normalized so that its total energy is 1, and $w(n)$, the channel noise, which, as in [35], we will approximate as AWGN.

The received signal gets equalized in order to compensate the ISI effects. We would have liked to use the DFE technique, but since we are in a pure analog framework, there is no quantization and hence, this method has been discarded in favor of linear MMSE. At the output of the equalizer, we obtain

$$u(n) = x(n) + w_q(n), \tag{4.1}$$

where $w_q(n)$ contains both the AWGN noise and the ISI contributions that have not been removed. In any case, we can approximate $u(n)$ with a Gaussian variable and define for every SNR (average power ratio between $x(n)$ and $w(n)$) a new equivalent SNR (average power ratio between $x(n)$ and $w_q(n)$). Thus we proceed as in the previous chapter and choose the non-linear curve parameters that are optimal for the new

equivalent SNR value.

### 4.3 Simulation Results

In this section we show the performance of our proposed system by simulating the transmission of a grayscale $256 \times 256$ pixel image [1] through the underwater acoustic channel. As for our joint source-channel encoder formed by the CS block and the non-linear mappings, three different system rates were used: 2:1, 4:1 and 8:1. For each case we tried both the 1:1 mappings and the 2:1 spiral mappings. Note that for the latter case the CS compression ratios are 1:1, 2:1 and 4:1, respectively.

Following the same method described in Section 3.5 we efficiently allocate energy to our channel symbols and we corrupt them by adding ISI and AWGN noise. The channel model used for our simulations was measured in a real experiment in the ocean by researchers of our University [42]. In a water depth region of 100 meters, source and receiver were separated 3 kilometers away. Using only a bandwidth of 8 kHz, the channel impulse response was measured and later resampled at 4, 6 and 8 kHz. Figure 4.2 (a) depicts the spread caused by the multipath effects. With the three profiles of $h(n)$ given to the receiver, the received symbols were equalized using a linear MMSE filter ten times the length of the impulse responses. Figure 4.2 (b) shows the performance for the three ISI channels by comparing their equivalent SNRs. Notice that while the 4 and 6 kHz ISI channels are able to follow the AWGN channel quite well, the 8 kHz ISI channel shows strong degradation due to its frequency nulls.

We decode our equalized symbols using the ML criterion. It is important to mention that the parameters used for both our analog encoder and decoder are the optimum ones for the equivalent SNR values after the equalization, not for the ones with just the AWGN noise. Finally, images are reconstructed and their SDR values are plotted as a function of the SNR over the different ISI channels. For comparison purposes, the results for AWGN are also shown. These results are presented in Figure 4.3.

[1] Picture of the Titanic wreck, courtesy of National Geographic.

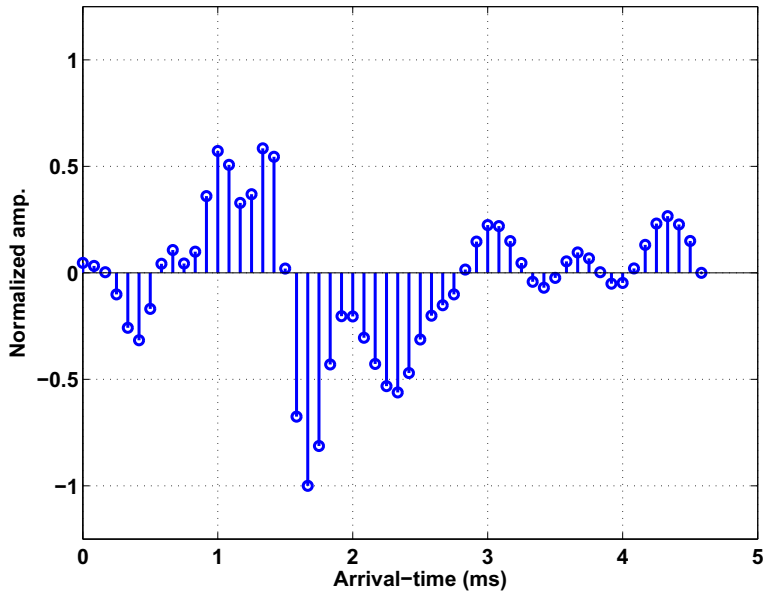


(a)

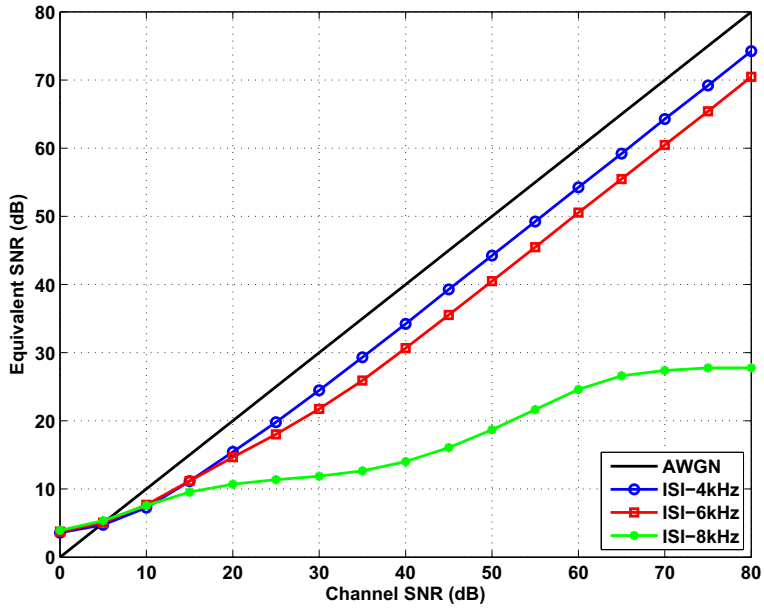


(b)

**Figure 4.2:** (a) Underwater channel's impulse response sampled at 12 kHz. (b) Equivalent SNR after equalization compared to the AWGN channel.

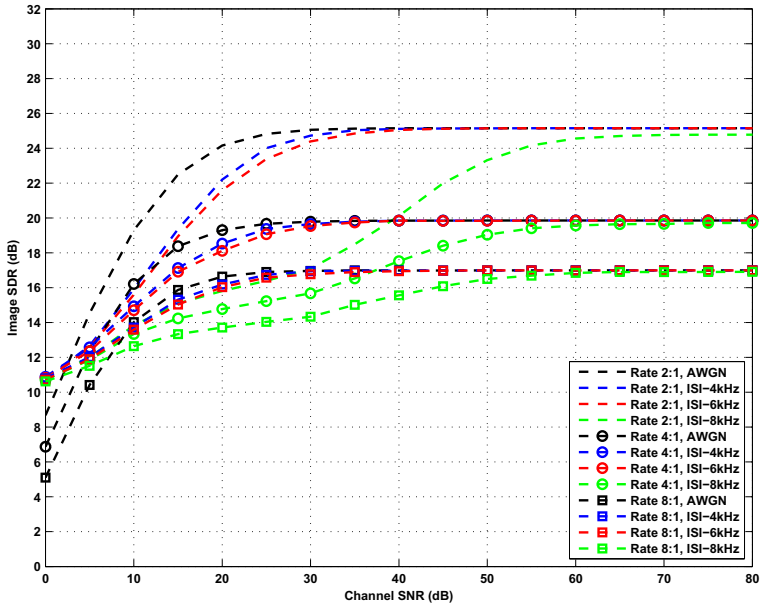


(a) 1:1 Mapping

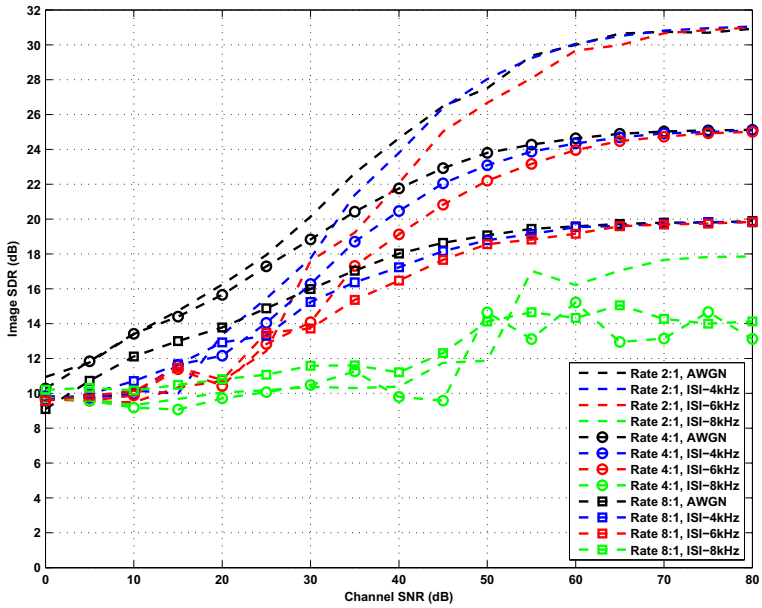


(b) 2:1 Mapping

**Figure 4.3:** Image SDR as a function of the channel SNR for different system rates and ISI channels using 1:1 non-linear mappings (a) or 2:1 spiral mappings (b).

Notice that in the cases of 4 and 6 kHz ISI channels the performance is very reasonable when compared to the AWGN channel with comparable CSNR. Other than

in the 2:1 system, the gap between them is quite tight, less than 1dB for most of the cases using 1:1 mappings and around 2-3 dBs when using 2:1 mappings. The case that behaves worst is the 8 kHz ISI channel, which is expected when we look at Figure 4.2 (b). For the 1:1 mappings, it takes around 30 extra dBs to catch up with the other ISI channels; and for the 2:1 mappings, it is never able to do so. Therefore, we would recommend its use only in speed critical applications. For the rest of the cases where we do not want to compromise performance, both the 4 and 6 kHz cases show satisfactory results.

It is important to realize that we can corroborate our discussion in Subsection 4.2.1 about where should redundancy be placed. For example, for the curve corresponding to the 4:1 system and 6 kHz ISI channel, notice how, for CSNRs above 40 dB, it is better to compress with the 2:1 mappings and use half the CS rate. Below that value, however, it is better to use 1:1 mappings and compress more with the CS block, since we know linear codes can be optimal at low CSNR regimes [32].

To complete our discussion, we include some image reconstructions over the 6 kHz ISI channel in Figure 4.4. For the three chosen CSNR values the pictures are totally recognizable and the great majority of the details are preserved. Furthermore, admitting we have a distorted reconstruction, if we make a simple calculation (8 bits/sample and 6000 symbols/second), it is straightforward to show that our transmission speed rates are of 96, 192 and 384 kbps for the 2:1, 4:1 and 8:1 system rates respectively. Recalling our image had $256 \times 256$ pixels (or samples), in each case, it would take us 5.46, 2.73 and 1.37 seconds to transmit it.

## 4.4 Conclusion

We have proposed a new image transmission system for acoustic underwater communications which, in contrast to the traditional digital approach, does not use bits at any moment and works only in the analog-amplitude discret-time domain. It consists of an all-analog joint source-channel encoder formed by a CS block and non-linear mappings that will generate the symbols to be transmitted through the

ISI channel. In order to improve performance, simulations show that the linear MMSE equalizer included at the receiver has critical importance. As far as received symbols are properly equalized, performance is very similar to the AWGN scenario and images can be transmitted with high speed and low complexity, allowing very tolerable distortion levels.

(a) Original image.

(b) 2:1 rate (1:1 mapping);
CSNR=15 dB; SDR=18.9 dB.

(c) 4:1 rate (2:1 mapping);
CSNR=40 dB; SDR=19.1 dB;

(d) 8:1 rate (2:1 mapping);
CSNR=45 dB; SDR=17.7 dB.

**Figure 4.4:** Reconstructed images over the 6 kHz ISI channel using different strategies.

# Chapter 5

# EXTENDED ANALOG MAPPINGS FOR NON-LINEAR AMPLIFIERS

In this chapter we investigate new analog mappings to overcome the non-linearities that may occur at the amplifying stage of our transmission system. Problems such as clipping are alleviated by using an extension of our space-filling curves that aims to match the pdf of our transmitted symbols with the channel statistics. For our analysis, we consider the case of 2:1 bandwidth reduction and a Gaussian source that produces i.i.d. samples. This will allow us to obtain the theoretical performance bounds and compare them with the results of our proposed framework. Simulations conclude that our time-discrete analog-amplitude communications system shows good behavior and successfully avoids the distortion introduced by the non-linear transducer for a wide range of signal to noise ratios.

## 5.1 Introduction

Most of the studies dealing with space filling curves [8], [36], [22] have been proposed for the case where the source produces Gaussian i.i.d. samples and the channel is AWGN. In our aim to extend the use of analog non-linear mappings to other scenarios, we consider the case where the amplifier at the transmitter introduces several non-linear distortions such as clipping or other undesired effects.

The motivation for this particular scenario comes from our experience in acoustic underwater communications, where it is often found that the transducer does not work in a perfectly linear regime and corrupts our signal with saturation effects. This phenomenon certainly modifies our channel model and the mappings designed for AWGN

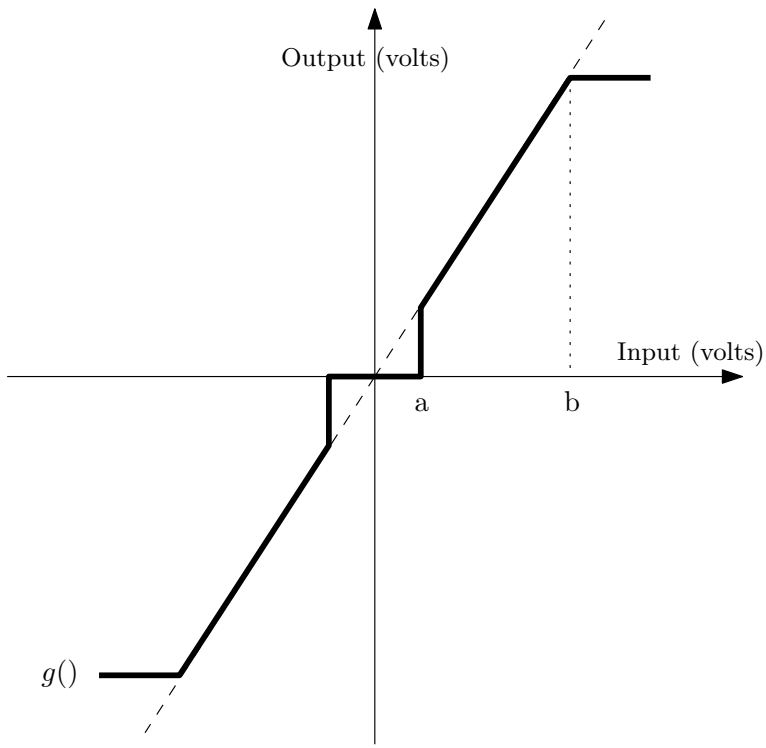


**Figure 5.1:** Amplifier introducing undesired non-linear effects.

channels would lead, in general, to suboptimal results. Therefore, new analog mappings need to be proposed in order to alleviate the distortion introduced by these non-linearities and perform closer to the theoretical limits.

In the next section we provide more details about the non-linear channel and, after that, we describe our proposed mapping. Next, we compare simulation results with the theoretically optimal performance. Finally, the last section presents our conclusions on this topic.

## 5.2 Non-Linear Channel Model

Figure 5.1 depicts the gain function $g()$ of the non-linear amplifier that we will consider. Compared to the ideal linear regime, the first irregularity is given by the values close to the origin. Notice how for inputs below $a$ volts the resulting output voltage is zero. The second constraint comes with the value of $b$ above which all input

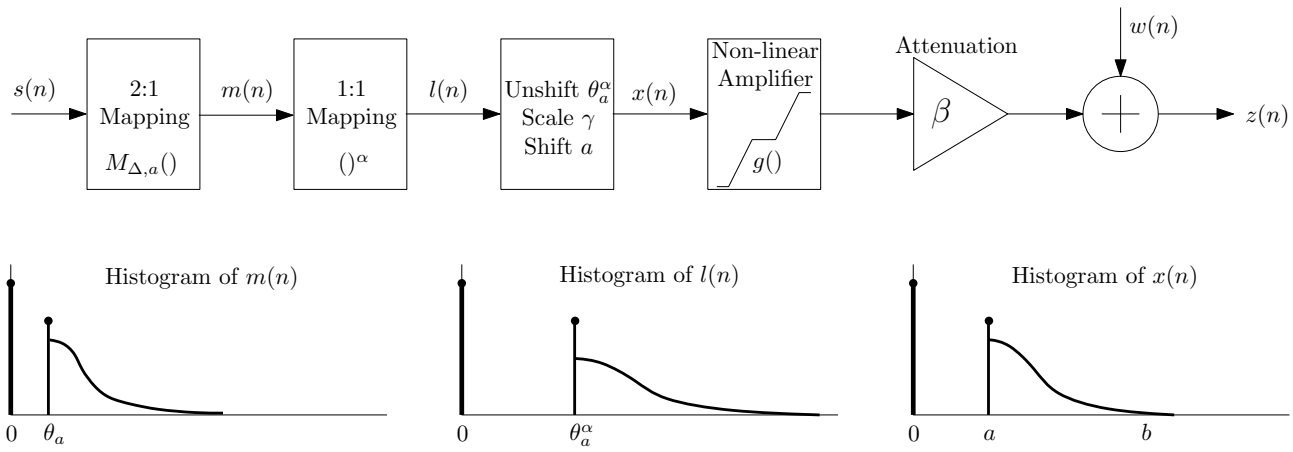


**Figure 5.2:** Proposed communication framework. Due to symmetry only right hand sides of the pdf functions are shown.

values are not correctly amplified but clipped to a saturation value $g(b)$. It is clear that this will limit our performance at low and high CSNR values.

The non-linearity in the amplifier brings up a very interesting idea about the channel model. Given that the AWGN noise that the receiver introduces is fixed, the CSNR depends on the attenuation and the signal level. Let us suppose we set a longer distance between transmitter and receiver and we still want to operate at the same CSNR: since the communication range has increased, so has the attenuation. Thus, in order to meet the CSNR requirement, we will need a higher energy level of our channel symbols $x(n)$; and here comes the key issue, as it may occur that channel symbols that were affected by the lower cut-off value $a$, now, due to increasing the communication distance, have their values above $a$ and are not distorted anymore. Alternatively, some channel symbols may be clipped. As a result of all this, in this channel model attenuation $\beta$ and noise $w(n)$ cannot be lumped together and the received symbols $z(n)$ are expressed as

$$z(n) = g(x(n)) * \beta + w(n). \tag{5.1}$$

## 5.3 Proposed System

Once we are familiar with the channel model we are facing, it is time to propose our design for a communication setup that can deal with all the mentioned problems. In Figure 5.2 we present the block diagram of a full analog communication system that uses a combination of space-filling curves as a joint source-channel encoder and a few simple shift and scale operations that aim to match the pdf of our channel symbols with the characteristics of our non-linear channel model.

The first block is based on the 2:1 Archimedean spiral that we presented in Equation 3.2 and also used in the previous chapter. However, this time the curve has been modified to mimic in some way the behavior of the non-linear amplifier. Now all the mapped symbols with absolute value below $\theta_a$, will experience a thresholding operation. If their absolute value is below $\theta_a/2$, they will be mapped to zero. Otherwise, they will be mapped either to $\theta_a$ or $-\theta_a$ according to their sign. This will allow us to have more control on which symbols are affected and avoid the undesired effects that the non-linear amplifier introduces.

The second block of our proposed system is the well known exponential mapping that we have used extensively since we presented it in Equation 3.3. It will change the energy distribution of our symbols with the goal of protecting them better from the channel noise.

Very simple shift and scale operations form our third block. Their purpose is basically fitting the pdf of our symbols between cutoff values $a$ and $b$, while also assigning the proper energy in order to meet the SNR value constraint. The overall system consists of three basic operations:

- Shifting down our non-zero values, so that the parts of the pdf that start at $\theta_a^\alpha$ and $-\theta_a^\alpha$ now begin at zero.
- Scaling all those symbols by a constant factor $\gamma$.
- Shifting up our values by $a$.

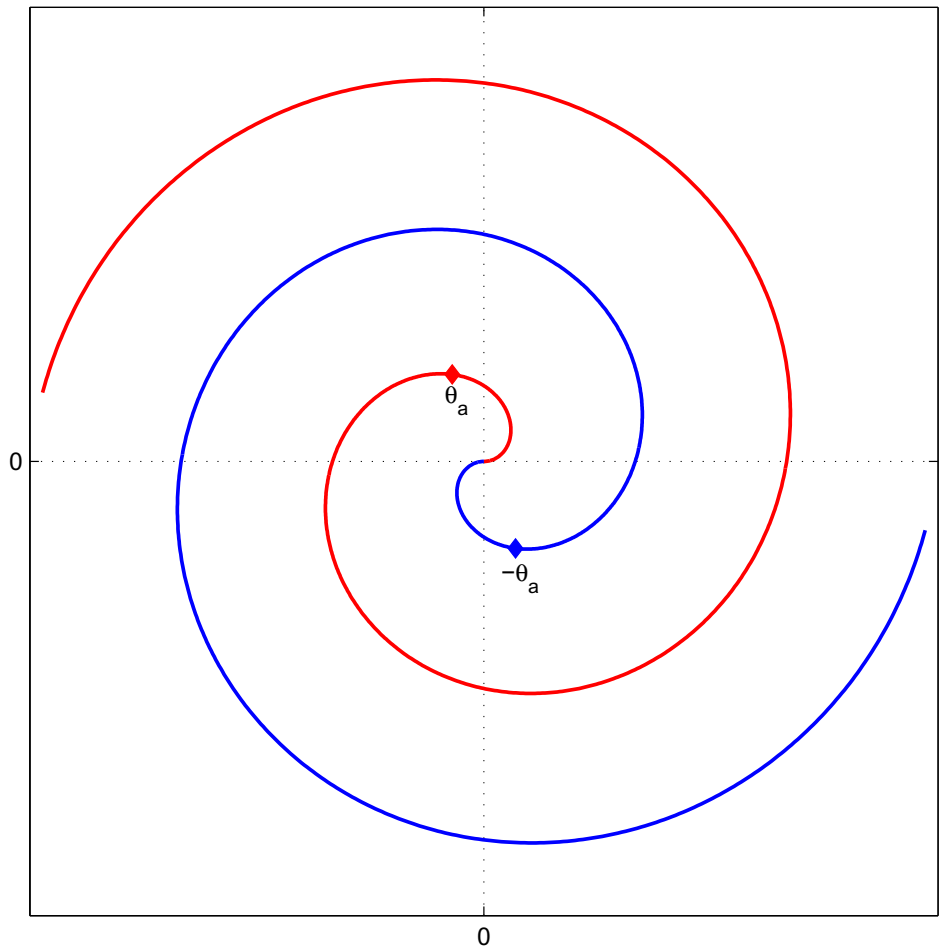


**Figure 5.3:** New 2:1 mapping with low cutoff values for both branches of the spiral.

Notice how, in Figure 5.2, our symbols $x(n)$ can now go through the non-linear amplifier (fourth block) with the problem of uncontrolled clipping greatly minimized.

By exploiting prior knowledge at the receiver side, we will apply thresholding at $a/2$ and also clip all the values above $b$. Later we will reverse the shift and scale operations previously described and use ML detection for both non-linear mappings. Notice that once again we have designed our communication system with a strong focus on low-complexity, a critical factor when one wants to maximize the autonomy of both transmitter and receiver.

## 5.4 Simulation Results

In order to show the effectiveness of the proposed system we have run simulations over a non-linear channel and compared them with other meaningful references. The channel model used for our calculations was obtained from [34] with the following system parameters: $a = 2$ volts, $b = 20$ volts, amplifier gain or slope= $\frac{1}{20}\sqrt{2 \cdot 10^{19}}$, attenuation for a 2 km communication distance $\beta = 62.46$ dB and noise variance at the receiver $\sigma_n^2 = 87.7$ dB.

First, with the goal of assessing a lower bound, we have considered the case where we do not take any protection measure against the non-linear effects introduced by the amplifier and run a standard 2:1 non-linear compression (Eq. 3.2) followed by a exponential 1:1 mapping (Eq. 3.3). The chosen $\Delta$ and $\alpha$ values are the optimal ones for ML detection, already calculated in [25].

Next, we simulate the case of our proposed system and find the optimal values for both $\Delta$ and $\alpha$. As for the value of our third parameter $\theta_a$ we add the following constraint $\theta_a^\alpha = a$. This means that in our mapping we are choosing the value of $\theta_a$ in a way that after the exponential 1:1 mapping the mapped symbols are already matching the amplifier's low cutoff value $a$. Although this criterion is simple and intuitive, in general, there is no guarantee of optimality. That is why our third simulation exploits that degree of freedom and optimizes for $\Delta$, $\alpha$ and $\theta_a$ at the same time. This requires

longer processing, but the good news is that the optimal values can be calculated once off-line and later used whenever they are needed.

Finally, we also include in our comparison two theoretical bounds obtained from [21]. The first one is based on the same non-linear channel model and the same system parameters here considered. Using the Blahut-Arimoto algorithm [2] the OPTA is calculated for this channel, which will be a great reference to compare our mappings with. In order to better contextualize this curve, the OPTA for the 2:1 compression in the AWGN channel is also included. This will give us an insight of how much the non-linearities are degrading our achievable performance.

All five mentioned curves can be seen in Figure 5.4. Notice that the CSNR value range is limited from around 5 to 35 dB due to the cut-off values of the amplifier. First, let us observe how the standard 2:1 mapping that does not make any extra consideration regarding the non-linear amplifier quickly gets stuck and performs far away from the rest of the curves for high CSNR. On the other hand, once we introduce the new 2:1 mapping, the available energy is more efficiently managed, and better results can be found for all the operative range: around 0.5 dB for low signal to noise ratios and up to 4 dB for high CSNR regimes. If we optimize over the third parameter $\theta_a$, the resulting improvement is not very significant, just less than 0.5 dB for a few CSNR values. Therefore, we can conclude that, in general, our initial rule of thumb $\theta_a^\alpha = a$ is good enough and that the extra complexity does not make for the achieved results. Finally, let us comment on the two theoretical bounds. For the low and mid CSNR region both curves stand pretty tight from each other but 3-5 dB above our mappings. Notice that we could decrease such a gap by using a MMSE decoder or a more sophisticated coding architecture (at the cost of increasing the complexity of our system). For high CSNR values, however, we can see that the OPTA for the non-linear channel also gets stuck and that our simple mappings perform rather well and come as close as 1.5 dB from the optimal performance. This means that our proposed system is a very good candidate under favorable conditions of noise and that it also clearly overperforms the previous standard mapping for all the cases with almost no extra

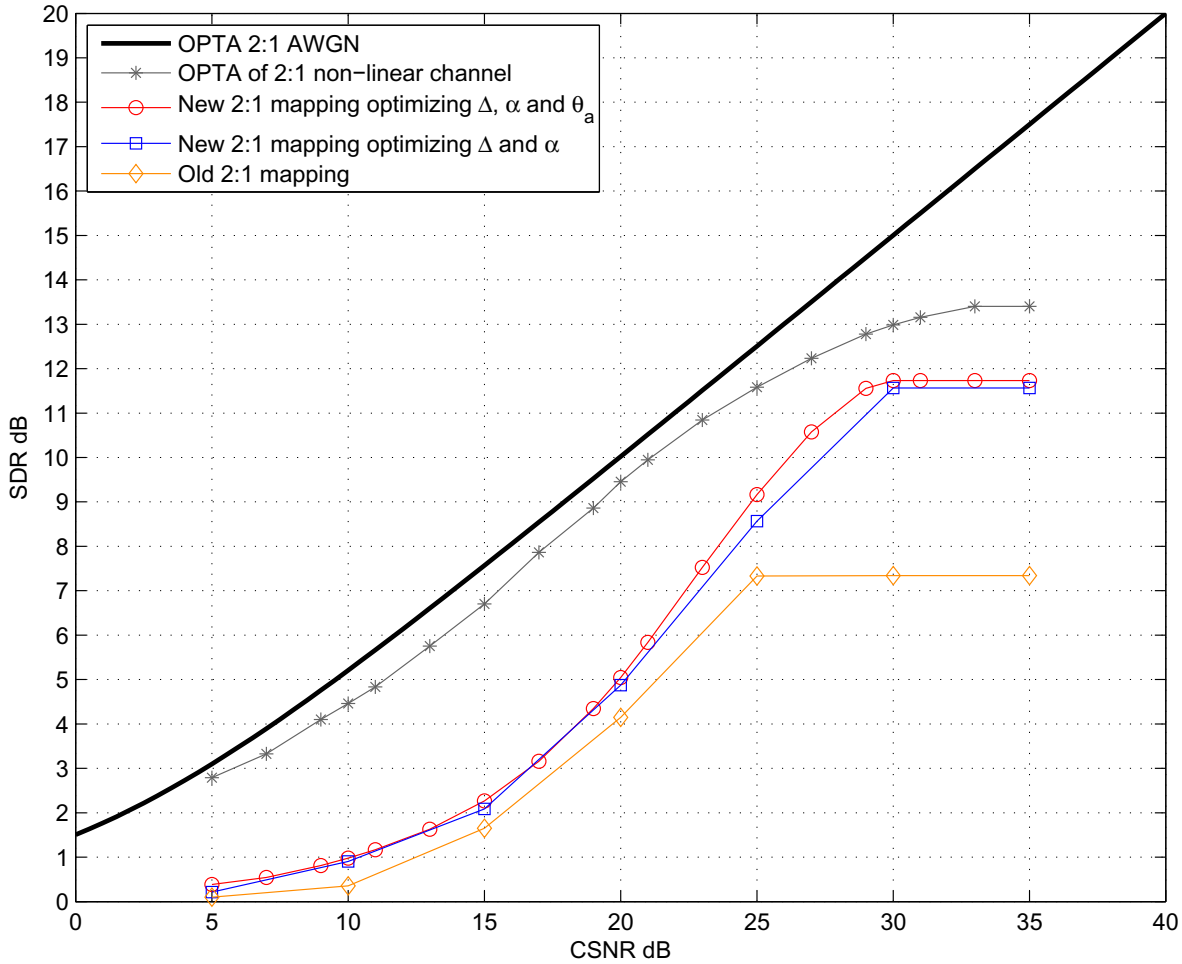


**Figure 5.4:** Simulation results for 2:1 compression using non-linear mappings over a non-linear amplifier.

complexity.

## 5.5 Conclusion

In this chapter we have presented an extension of space-filling curves for non-linear channel models often encountered in the amplifiers of underwater acoustic communications. By incorporating a cutoff value in the standard 2:1 spiral mapping and optimizing the parameters of the analog encoder block, we can avoid the non-linear distortions introduced at the amplifying stage. The results obtained at high CSNR region are excellent and the performance for other CSNR values is still better than when using the standard 2:1 mapping. Still, the gap between the OPTA and our proposed curves could be decreased by introducing more complex communication codes, which goes beyond the goals of this thesis.

# Chapter 6

# CONCLUSIONS AND FUTURE RESEARCH

In this thesis we have investigated several extensions for a very promising family of communication codes: non-linear space-filling curves for time-discrete and amplitude-continuous sources. Disregarding the traditional digital approach that assumes infinite block-lengths and very large complexity, we have focused on finding new mappings and scenarios for this particular kind of systems that work surprisingly close to the optimal performance using very little processing resources and adding no delay at all.

Specifically, in Chapter 3 we drastically decreased complexity and proposed a better energy allocation method for transmitting CS images through an AWGN channel. In Chapter 4 we took the same communication system a step further and extended it to ISI channels by adding an equalizing stage to our block diagram. Simulation results were really encouraging and suggested that new undersea expeditions could easily transmit underwater images with our proposed technology. In Chapter 5 we gave an alternative to a problem usually found in underwater acoustic communications: non-linear effects introduced at the amplifying stage. By designing a new 2:1 mapping that incorporates the non-linear effect itself, we managed to have better control over the distortion and improved the performance of standard 2:1 mappings by more than 3 dB for high CSNR regimes.

To conclude this work, we would like to point out other research topics that, in our opinion, would greatly contribute to further extending the use of analog mappings in communications. For example, developing simple codes for higher compression ratios such as 4:1, 8:1, 16:1 etc. As the number of involved dimensions increases, the

projection operation becomes harder and harder to calculate and more research on this topic is necessary.

Another interesting idea that we have not considered in this thesis is expansion ratios (e.g. 1:3). Such codes could enable the next generation of communication systems with much more autonomy and the same quasi-optimal performance.

Finally, we believe this research field could benefit very much from more theoretical analysis for the mappings and, equally important, for the achievable performance limits. Let us recall that our mappings focus on low complexity and had block-lengths of 1, while the OPTA curves used all along this thesis assume boundless complexity and infinite block-lengths.

## BIBLIOGRAPHY


[1] R. Baraniuk, "Compressive sensing," *IEEE Signal Processing Magazine*, vol. 24, no. 4, pp. 118-121, July 2007.

[2] R. Blahut, "Computation of channel capacity and rate-distortion functins," *IEEE Trans. on Information Theory*, vol. 18, no. 4, pp. 460–473, July 1972.

[3] E. Candes and J. Romberg "Sparsity and incoherence in compressive sampling," *Inv. Probl*, vol. 23, no. 3, pp. 969-985, 2007.

[4] E. Candes, J. Romberg, and T. Tao, "Robust uncertainty principles: exact signal reconstruction from highly incomplete frequency information," *IEEE Trans. on Information Theory*, vol. 52, no. 2, pp. 489-509, February 2006.

[5] E. Candes, J. Romberg, and T. Tao, "Stable signal recovery from incomplete and inaccurate measurements," *Communications on Pure and Applied Mathematics*, vol. 59, no. 8, pp. 1207-1223, August 2006.

[6] E. Candes and T. Tao, "Near optimal signal recovery from random projections: universal encoding strategies?," *IEEE Trans. on Information Theory*, vol. 52, no. 12, pp. 5406-5425, December 2006.

[7] S. S. Chen, D. L. Donoho, and M. A. Saunders,"Atomic decomposition by basis pursuit," *SIAM SCI. Comput.*, vol 20, no. 1, pp. 33-61, August 1998.

[8] S. -Y. Chung, "On the construction of some capacity-approaching coding schemes," *Ph.D. Thesis, Massachusetts Institute of Technology*, 2000.

[9] R. F. W. Coates, M. Zheng, and L. Wange, "'BASS 300 PARACOM': A 'model' underwater parametric communication system," *IEEE J. Ocean. Eng.*, vol. 21, no. 2, pp. 225–232, Apr. 1996.

[10] D. Donoho, "Compressed sensing," *IEEE Trans. on Information Theory*, vol. 52, no. 4, pp. 1289-1306, April 2006.

[11] R. L. Eastwood, L. E. Freitag, and J. A. Catipovic, "Digital acoustic telemetry of color video information," in *Proc. Oceans*, Ft. Lauderdale, FL, Sept. 1996, pp. 63–68.

[12] M. Elad, "Optimized projections for compressed sensing," *IEEE Trans. on Signa Processing,* vol. 55, no. 12, pp.5695-5702, December 2007.

[13] I. Esnaola and J. Garcia-Frias, "Exploiting prior knowledge in the recovery of non-sparse signals from noisy random projections," *Proc. CISS'07*, March 2007.

[14] P. A. Floor and T. A. Ramstad, "Dimension Reducing Mappings in Joint Source-Channel Coding," *Proc. NORSIG*, June 2006.

[15] A. Fuldseth and T. A. Ramstad, "Bandwidth compression for continuous-amplitude channels based on vector approximation to a continuous subset of the source signal space," *Proc. ICASSP'97*, April 1997.

[16] L. Gan, T. T. Dao, and T. D. Tran, Fast compressive Imaging Using Scrambled Block Hadamard Ensemble, preprint, 2008.

[17] M. Gastpar, "To code or not to code," *Ph.D. Dissertation, Ecole Polytechnique Federale (EPFL)*, Lausanne, Switzerland, 2002.

[18] M. Gastpar, B. Rimoldi, and M. Vetterli, "To code, or not to code: lossy source-channel communication revisited," *IEEE Trans. on Information Theory*, vol. 49, no. 5, pp. 1147-1158, May 2003.

[19] M. Gastpar and M. Vetterli, "Source-channel communication in sensor networks," *Information Processing in Sensor Networks*, Springer Berlin, 2003.

[20] T. Goblick, "Theoretical limitations on the transmission of data from analog sources," *IEEE Trans. on Information Theory*, vol. 11, no. 4, pp. 558-567, October 1965.

[21] M. Hassanin and J. Garcia-Frias, "Analog joint source channel coding over non-linear acoustic channels", *Proc. CISS'13*, March 2013.

[22] F. Hekland, G. E. Oien, and T. A. Ramstad, "Using 2:1 Shannon mapping for joint source-channel coding," *Proc. DCC'05*, March 2005.

[23] D. F. Hoag, V. K. Ingle, and R. J. Gaudett, "Low-bit-rate coding of underwater video using wavelet-based compression algorithms," *IEEE J. Ocean. Eng.*, vol. 22, no. 2, pp. 393–400, Apr. 2008.

[24] Y. Hu, "Analog non-linear coding for improved performance in Compressed Sensing," *M.Sc. Thesis, University of Delaware*, 2009.

[25] Y. Hu, J. Garcia-Frias, and M. Lamarca, "Analog joint source-channel coding using space-filling curves and MMSE decoding," *Proc. DCC'09*, March 2009.

[26] Y. Hu, Z. Wang, J. Garcia-Frias, and G. R. Arce, "Non-Linear Coding for Improved Performance in Compressive Sensing," *Proc. CISS'09*, March 2009.

[27] I. Iglesias, B. Lu, J. Garcia-Frias, and G. R. Arce, "Non-linear mappings for transmission of compressed sensing images," *Proc. Allerton'10*, September 2010.

[28] I. Iglesias, A. Song, J. Garcia-Frias, M. Badiey, and G. R. Arce, "Image transmission over the underwater acoustic channel via compressive sensing," *Proc. CISS'11*, March 2011.

[29] D. B. Kilfoyle and A. B. Baggeroer, "The state of the art in underwater acoustic telemetry," *IEEE J. Oceanic Eng.*, vol. 25, no. 1, pp. 4–27, Jan. 2000.

[30] Y. Kochman and R. Zamir, "Analog matching of colored sources to colored channels," *Proc. ISIT'06*, July 2006.

[31] V. A. Kotel'nikov, "The theory of optimum noise immunity," *New York: McGraw-Hill*, 1959.

[32] K.-H. Lee and D. P. Petersen, "Optimal linear coding for vector channels," *IEEE Trans. on Communications*, vol. 24, no. 12, pp. 1283-1290, December 1976.

[33] LinkQuest, Inc., "Underwater acoustic modems," online, http://www.linkquest.com/html/uwm_hr.pdf.

[34] D. Lucani, M. Stojanovic, and M. Medard, "On the relationship between transmission power and capacity of an underwater acoustic communication channel," *OCEANS 2008 - MTS/IEEE Kobe Techno-Ocean*, pp. 1–6, April 2008.

[35] J. C. Preisig, "Performance analysis of adaptive equalization for coherent acoustic communications in the time-varying ocean environment," *J. Acoust. Soc. Am.*, vol. 118, no. 1, pp. 263–278, Jul. 2005.

[36] T. A. Ramstad, "Shannon mappings for robust communication," *Telektronikk*, vol. 98, no. 1, pp. 114-128, 2002.

[37] J.K. Romberg, H. Choi, and R. G. Baraniuk, "Bayesian tree-structured image modeling using wavelet-domain hidden Markov models," *IEEE Trans. Image Process.,* vol. 10, no. 7, pp. 1056-1068, Jul. 2001.

[38] S. Roy, T. M. Duman, V. McDonald, and J. G. Proakis, "High rate communication for underwater acoustic channels using multiple transmitters and space-time coding: Receiver structures and experimental results," *IEEE J. Oceanic Eng.*, vol. 32, no. 3, pp. 663–688, Jul. 2007.

[39] C. E. Shannon, "A mathematical theory of communication," *The Bell System Technical Journal*, 27:379-423, 1948.

[40] C. E. Shannon, "Communication in the presence of noise," *Proc. IRE*, vol. 37, pp. 10-21, January 1949.

[41] C. Schróder, P. Bórnert, and B. Aldefeld, "Spatial excitation using variable-density spiral trajectories," *J. Mag. Reson. Imag.,* vol. 18, no. 1, pp. 136-141, 2003.

[42] A. Song, M. Badiey, H.-C. Song, W. S. Hodgkiss, M. B. Porter, and the KauaiEx Group, "Impact of ocean variability on coherent underwater acoustic communications during the Kauai experiment (KauaiEx)," *J. Acoust. Soc. Am.*, vol. 123, no. 2, pp. 856–865, Feb. 2008.

[43] H.C. Song, W.S. Hodgkiss, W.A. Kuperman, T. Akal, and M. Stevenson, "High-frequency acoustic communications achieving high bandwidth efficiency (L)," *J.Acoust. Soc. Am.*, vol. 126, no. 2, pp. 561–563, Aug. 2009.

[44] M. Stojanovic, J. A. Catipovic, and J. G. Proakis, "Adaptive multichannel combining and equalization for underwater acoustic communications," *J. Acoust. Soc. Am.*, vol. 94, no. 3, pp. 1621–1631, Sept. 1993.

[45] M. Stojanovic, J. A. Catipovic, and J. G. Proakis, "Phase-coherent digital communications for underwater acoustic channels," *IEEE J. Oceanic Eng.*, vol. 19, no. 1, pp. 100–111, Jan. 1994.

[46] Z. Wang and G. R. Arce, "Variable density compressed image sampling," *IEEE Trans. on Image Processing*, vol. 19, no. 1, pp. 264-270, Jan 2010.

Aquí no valen dotores,
sólo vale la esperiencia;
Aquí verían su inocencia
ésos que todo lo saben
porque esto tiene otra llave
y el gaucho tiene su cencia.

*El Gaucho Martín Fierro*